A NANO-SIZED APPROACH AT EXPLOITING THE PANCREATIC TUMOR MICROENVIRONMENT

A Dissertation
Submitted to the Graduate Faculty
of the
North Dakota State University
of Agriculture and Applied Science

By

Matthew Ian Confeld

In Partial Fulfillment of the Requirements
for the Degree of
DOCTOR OF PHILOSOPHY

Major Department:
Pharmaceutical Sciences

November 2019

Fargo, North Dakota

North Dakota State University
Graduate School

Title

A Nano-Sized Approach at Exploiting the Pancreatic Tumor Microenvironment

By

Matthew Ian Confeld

The Supervisory Committee certifies that this ***disquisition*** complies with North Dakota State University's regulations and meets the accepted standards for the degree of

DOCTOR OF PHILOSOPHY

SUPERVISORY COMMITTEE:

Sanku Mallik
Chair

Amanda Brooks

Kristine Steffen

Mohiuddin Quadir

Approved:

4/20/2020
Date

Jagdish Singh
Department Chair

ABSTRACT

Just 3% of all new cancer cases in the United States are pancreatic. Yet, pancreatic cancer continuously is shown to be one of the most lethal and common causes of cancer death. Early detection is critical. However, oncologists and researchers have struggled to find effective strategies or tests to detect cancer of the pancreas early on in development. Thus, the cancer is often found late stage and requires significant chemotherapy intervention. These multi-drug treatment cocktails have shown benefit, but only add a few months to a patient's life. Significant adverse effects often limit the full effective doses of treatment. In order to limit these adverse effects, as well as increase the effectiveness of treatment, we have designed, optimized, and tested unique drug carriers known as polymersomes. Using characteristics of the environment surrounding pancreatic tumors and the cells found therein, we created targeted therapies that are responsive and relatively selective toward cancerous cells. Herein, are found two distinct polymersomes. The first, is a oxygen reactive drug carrier with an additional small peptide molecule that is able to penetrate dense tumor tissue and has shown decreased tumor growth of 260% as compared to control samples in an animal model of pancreatic cancer. The chemical make-up of this polymersome allows for extended circulation time and a high accumulation at the tumor site. A second design, uses an intracellular enzyme to destabilize the polymersomes' structure, which in turn, releases a selected chemotherapy drug near its intended site of action. This strategy, has shown a 10 fold increase in potency of the chemotherapy drug, as compared to when the drug is given alone and showed decreased toxicity to non-cancerous cells. It is certain that thoughtful drug delivery strategies and not just drug molecule design will be instrumental in the paradigm shift of pancreatic cancer from likely death to survival.

TABLE OF CONTENTS

LIST OF TABLES

Table Page

LIST OF FIGURES

LIST OF SCHEMES

LIST OF APPENDIX FIGURES

A MICRO HISTORY OF NANOMEDICINE

We can trace our earliest medicines and remedies back over 4,500 years ago. The ancient Egyptians used a wide assortment of herbs, plants, and even bones. Using the technology and understanding they had, they were able to produce modest effects in therapy. Of course, there would have been a substantial amount of trial and error and not everyone was lining up for treatments that included animal feces or ingesting metals. Over time, the understanding of medicine increased, and we began to develop a better knowledge of the human body's complex biology. The Greek, Diocles, wrote the first known book of anatomy in 300 BC followed by Pedanius Dioscorides, who wrote the book De Materia Medica in 60 AD. De Materia Medica included herbal medicines, medicinal substances and later became a leading pharmacological text for the next 1,500 years. Countless other scientists have given their lives to bettering the human condition; from producing the first vaccines to solving the structure of DNA. However, over 500,000 people still die in the United States each year from a malignant group of diseases known as cancer. Even with 4,500 years of medical knowledge and experimentation we are still often baffled by this disease. Thousands of new and experimental drugs have been trialed. Yet, only 1 in 50 will make it to market. Many times, these new drugs fail. Most often due to intolerable toxicity, solubility, or lack efficacy. What if, it is not the drug itself that is the problem? What if, the problem is delivery?

While not nearly as old as Egyptian medicine, nanomaterials are a relatively new field that has applications across many disciplines. Nanomedicine is the use of nanomaterials for medical purposes. The history of nanomedicine starts in 1954, with a German scientist publishing the first reported polymer-drug conjugate.[1] Soon thereafter, another group discovered liposomes, a lipid based nanoparticle.[2]A third major type of nanoparticle based on albumin was

produced by Scheffel and team in 1972.[3] The final piece of the nanoparticle puzzle was the observation of an enhanced accumulation of nanoparticles at the tumor site brought on by altered tumor vasculature.[4] This finding went on to become a major concept in cancer nanomedicine known as the enhanced permeability and retention (EPR) effect. These breakthroughs, among others, eventually led to the formulation and FDA approval of the first nanoparticle for cancer treatment in 1995. Doxil, a liposomal nanoparticle, encapsulated the previously FDA approved anticancer drug doxorubicin and led to a significant reduction in toxic adverse effects. Ten years later, an albumin bound nanoparticle drug formulation (Abraxane) was approved that removed the need for organic solvents during administration, preventing solvent-related side effects. There are now over 50 nanopharmaceuticals approved by the FDA for various disease states.[5] However, we are just scratching the surface of the possibilities these particles have. Research is being conducted to make nanoparticles in many sizes, shapes, targeting moieties, externally responsive (ultrasound, magnetism, light etc.) and even able to be responsive to the tumor's own microenvironment.

The Tumor Microenvironment

The focus of this research is to take advantage of specific abnormal characteristics of the pancreatic tumor microenvironment (TME). To do this, we must first understand the microenvironment itself. The pancreatic tumor microenvironment is not simply a mass of malignant aggressive atypical cells but rather a combination of fibroblasts, adipocytes, extracellular matrix, endothelial cells, hematopoietic cells, stromal cells, and stem or stem-like cells.[6–8] Furthermore, cells are not stagnant. They are replicating, initiating cell-death mechanisms, and secreting many components that further modify the TME. Sometime during early carcinogenesis, fibroblasts begin to secrete large amounts of proteins necessary for

extracellular matrix (ECM) formation, namely laminins, fibronectins, and collagens.[9] This leads to a desmoplastic stroma, which acts as a shelter for the tumor. Release of various chemokines and continued release of ECM proteins provides immune evasion, promotion of migration, and inhibition of angiogenesis, in turn creating hypovascular hypoxic niches. The lack of vasculature and blood flow, makes getting effective concentrations of chemotherapy to the tumor difficult. Chemotherapeutic agents must travel through a biological maze to reach their site of action. Chemically modified nanoparticles can exploit an intrinsic cellular function known as macropinocytosis as a way of "cheating" these biological mazes and reach the hypoxic hypovascular niches.

Histone deacetylase (HDAC) proteins are one of multiple proteins that play a significant role in transcription. An apparent over expression of specific HDACs namely 1, 7, and 8 is observed in many pancreatic cancer patients.[10] The downstream role that these enzymes play in altering cellular function and overall tumor microenvironment is not fully understood. The theorized implications are: a lack of inactivated genes and/or over inactivation of genes involved in proliferation, apoptosis, and immune suppression. High levels of HDACs correlated with significantly worse overall patient survival, hinting to a potentially important transcriptional role in pancreatic cancer.

Designing and Optimizing Polymeric Nanoparticles

Medicinal chemistry has played a significant role in an often-overlooked aspect of medicine, formulation. Small alterations to a chemical structure can greatly increase or decrease the effectiveness of a drug. Parameters such as, solubility, pH, size, stability, and even dosage form (i.e. capsule, tablet, solution), can make an impactful difference when it comes to FDA approval and efficacy in general. Formulation and design must be thoughtfully carried out for

nanoparticles as well. Detailed below are three important design principles for polymer nanoparticles that will increase their translational potential.

The general objective in designing nanoparticles is the delivery of a selected therapeutic agent (small molecule, proteins, nucleic acids, etc.). Accomplishing this objective often comes down to knowing the chemical characteristics of the therapeutic agent with emphasis on molecular charge and solubility. While it is possible to design nanoparticles around a specific drug, it is more lucrative to design a particle that is non-specific for the encapsulated contents. This is important for cancer therapeutics, as multi-drug treatment strategies are becoming common. Drug/therapeutic agent(s) selection should use evidence-based results either in-vivo or in-vitro.

Design Principle 1: Material Selection

One of the guiding theories for the use of nanomedicine is the potential for reduced side effects while maintaining or increasing efficacy. Doxil™, the nanoparticle formulation of doxorubicin was one of the first clinical attempts at testing this hypothesis. Many studies and thousands of patients lead us to believe it has been successful, as pooled-analysis show significant decreases in adverse events while keeping similar efficacy.[11] Nanoparticle material selection is a key parameter controlling these results. The terms bio-compatible, bio-degradable, and non-toxic are often used in describing these materials that are often made from simple molecules. The polymers are composed of monomers that are naturally produced or easily broken down by the body. The most commonly used polymeric materials are: polylactic acid (PLA), a polymer composed of lactic acid, the same molecule produced by our muscles during exercise. Poly lactic-co-glycolic acid (PLGA) is composed of PLA and glycolic acid; this polymer undergoes hydrolysis in the body to produce lactic acid and glycolic acid (a metabolic

by-product) that is easily metabolized and excreted. The third most common polymer is polyethylene glycol (PEG), which goes through multiple metabolic transformations in the liver producing glycoaldehyde, glycolic acid, and other minor compounds. Regardless of the selected polymer, cellular toxicity should be determined early.

Design Principle 2: Minimize Polymer Toxicity and Immune Response

The next principle accounts for the body's action on nanoparticles. The first challenge encountered by nanoparticles is the mononuclear phagocyte system (MPS). This is the body's way of removing foreign particles/materials out of the blood stream. Macrophages, a phagocytic cell found within tissues and blood, recognize nanoparticles as foreign and in turn, attempt to engulf them. Macrophages use an array of enzymes to break down whatever it has ingested. To counter these phagocytic cells, PEG coatings can be applied to the nanoparticles. This coating creates a brush border that is able to prevent opsonization coating by antibodies, a method used by our body to target molecules, bacteria, or nanoparticles for removal by the macrophages.[12–14]

The bodies complement system, named in part to its enhancement of our immune system functioning, consists of small proteins that circulate in the blood. Once the complement system is triggered, it initiates the release of cytokines leading to stimulation of phagocytes and increased inflammation to attract additional phagocytes. A highly complex and intricate system that includes over 30 small proteins has potential for creating lethal outcomes if over activation occurs. These proteins along with many others flowing through our plasma create a biological shell termed the protein corona. This corona consists of proteins bound to the nanoparticle, the hard shell, and proteins bound to those proteins which adsorb and desorb sporadically. The affinity and amount of protein absorbed is highly dependent on polymer composition and surface chemistry.[15] In general, hydrophobic particles provide enhanced absorbability of plasma proteins

leading to increased destruction and uptake by the immune system where hydrophilic particles have lessened absorbability.[16] While certain interpatient genetic difference can contribute to the level of complement response, there is currently no proven method for predicting a patient's response to a foreign nanomaterial. Further adding complexity to nanoparticle design, is that we often see difference between in-vitro immune responses and those that occur in-vivo.[17] The potential for life-threatening immune reactions is real and caution should be taken when using nanoparticles in treatment naïve patients. Current and future nanomedicine research is working towards immune neutral particles. Variation in molecular features including; surface charge, corona molecules, size, shape, and materials, may hold promise in reaching neutrality.[18–20]

The kidneys are the primary filtration center in our bodies, processing 180 liters of fluid per day. Filtration is carried out by a size and charge regulated membrane. Small pore sizes of about 10 nm within the kidneys are relatively impervious to particles larger than 100 nm. With multiple negatively charged layers, the kidney exhibits charge dependent filtration that induces clearance in a charge dependent manner. The fastest clearance is seen with positively charged particles and slowest clearance by negatively charged molecules.[21]

The final major obstacle for clinical use of nanoparticles is the liver. This organ is the major filter for our bodies and consequently most implicated in removal of nanoparticles. There is a significant decrease in blood flow going through the liver, which is thought to increase nanoparticle interaction with hepatic cells, leading to their removal.[22] While ideas have been proposed, such as, increasing liver blood flow or altering phenotypes to prevent nanoparticle uptake, there is currently no guaranteed strategy for bypassing liver uptake. The current best strategy to prevent significant alteration of pharmaceuticals is to inject them via the intravenous route. This allows for the by-pass of the liver's initial 1st pass metabolism.

Design Principle 3: Particle Size

Accounting for these design principles has led to many studies manipulating nanoparticle materials, sizes, and chemistry in order to find ideal characteristics.[23–30] Further advancements have led to a new generation of materials, referred to as "smart" polymers. These smart polymers create nanoparticles that are responsive to outside stimulus, creating a selective release mechanism. The nanoparticles we designed and tested take into account the initial three design principles (material, toxicity, and size) as well as use of smart polymers for specific release of contents. The first design incorporates a 4,4' azobenzene linker, creating a hypoxia responsive polymer (Chapter 2).[31,32]

The second design creates a dual-functional nanoparticle. Here, a PEG shell is utilized to discourage immune cell uptake and increase circulation time. This design utilizes an enzyme targeting/inhibitory strategy in addition to encapsulated drug delivery. As the nanoparticles find their way to the tumor microenvironment, they encounter altered expression of histone deacetylase (HDAC) enzymes. These HDAC enzymes, which are responsible for regulating gene transcription, bind to the nanoparticles. These nanoparticles act as a substrate for the HDAC enzymes active site. This has two outcomes: the nanoparticle's acetylated lysine residues are deacetylated and destabilized releasing the chemotherapeutic agent inside. The second outcome is that simultaneously the nanoparticles are occupying the HDAC enzyme and preventing it from completing its role in controlling DNA epigenetics and regulation (Chapter 3).

We created polymeric nanoparticles using the aforementioned design principles. Through testing and optimization we found these nanoparticles to be stable and able to encapsulate chemotherapeutic cargo. We hypothesized that these nanoparticles will be able to increase the efficacy of chemotherapeutics compared to unencapsulated therapies.

Hypoxia-Responsive Nanoparticles: AIMs

- Prepare multi-modal polymersomes that are hypoxia responsive and targeted towards pancreatic cancer cells.
- Demonstrate efficacy of polymersomes vs. unencapsulated drug under normal and hypoxic conditions in-vitro.
- Utilize a mouse model of pancreatic cancer and compare efficacy of polymersomes vs. unencapsulated drugs.

HDAC-Responsive Nanoparticles: AIMs

- Prepare polymersomes that utilize HDAC enzyme mediated release.
- Demonstrate efficacy of polymersomes vs. unencapsulated drug in-vitro.

TARGETING THE TUMOR CORE: HYPOXIA RESPONSIVE NANOPARTICLES FOR DELIVERY OF CHEMOTHERAPY TO PANCREATIC TUMORS

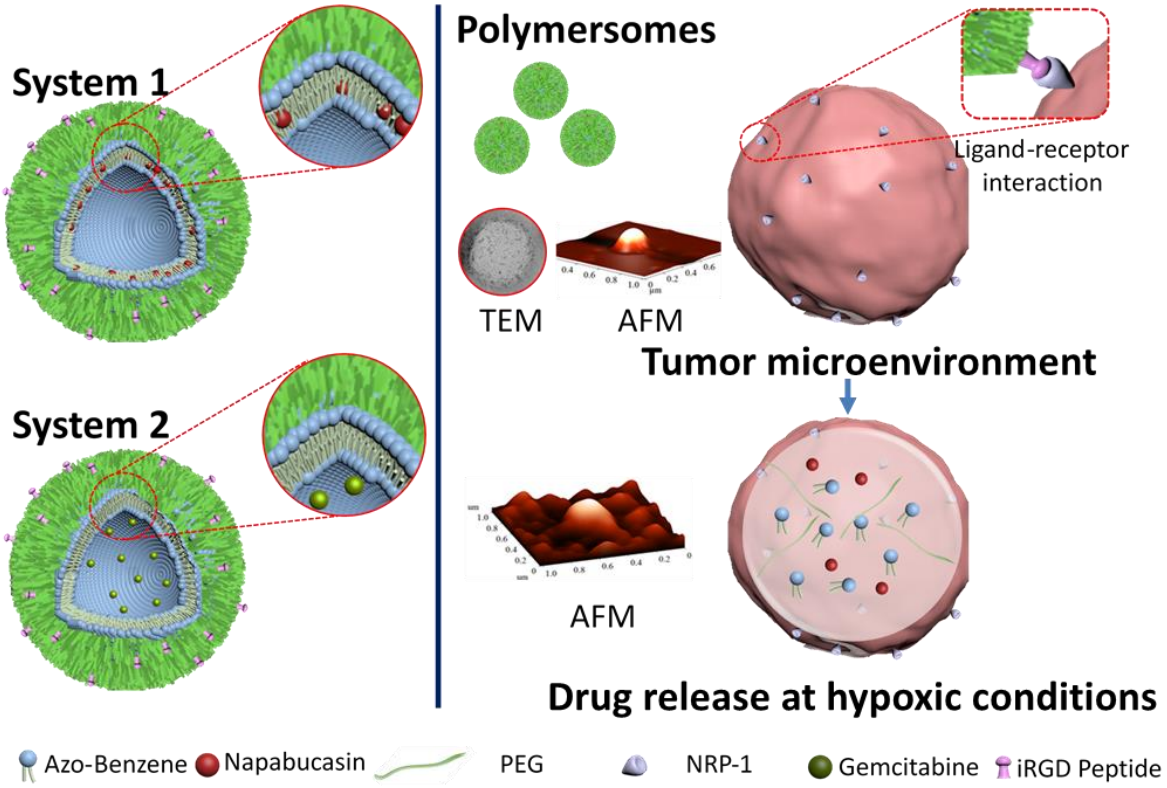

Figure 1. Hypoxia Responsive Nanoparticles Illustration.

Abstract

Oxygen is a necessary component of our daily lives both macroscopically and microscopically. However, cancer cell populations have the ability thrive and mutate in oxygen depleted environments. Chronic hypoxia, found in many solid tumors, alters cellular gene expression; thereby, altering signaling pathways that modulate proliferation, angiogenesis, and apoptosis. In pancreatic ductal adenocarcinoma (PDAC), early onset of hypoxia triggers remodeling of the extracellular matrix, epithelial-to-mesenchymal transition, increased cell survival, and metastasis. Specifically, cancer stem cells, are thought to contribute to metastasis, drug resistance, and relapse, resulting in a grim prognosis evident by 5-year survival rate of only

8%. In addition, hypoxia in PDAC is associated with the development of collagen-rich, fibrous extracellular stroma (desmoplasia) that makes it difficult for therapy to penetrate the tumor.

To overcome these daunting challenges, we created polymer nanoparticles (polymersomes), which target and penetrate pancreatic tumors, resulting in structural destabilization and release of encapsulated payloads in response to hypoxia. We successfully delivered a chemotherapeutic payload deep into the hypoxic niches of solid pancreatic tumors using uniquely designed polymersomes containing a hypoxia responsive linker and a tumor penetrating peptide. In vitro studies indicated a high cellular uptake of the polymersomes and an increased cytotoxic effect of our chemotherapy drugs (napabucasin and gemcitabine) under hypoxic conditions compared to unencapsulated drugs. Our animal study found polymersome formulations effectively decreased tumor growth by 260%, as well as, increased necrosis within the tumor core by 60% as compared to untreated controls. Therefore polymersomes showcase a therapeutic advantage over unencapsulated drugs that warrants further investigation for treatment of solid tumors.

Introduction

Solid tumors account for roughly 85% of all human cancers.[33] While surgical resection is often the most effective treatment procedure, it is not always possible or practical depending on the type and location of the tumor. Thus, an anticancer drug(s) is the primary treatment option in many cases. The success of each drug largely depends on efficient delivery to the tumor site, ideally with as little offsite toxicity as possible. Not surprisingly, even the best clinical chemotherapy agents are ineffective if they are unable to reach their intended site of action. For example, a drug given intravenously will concentrate in areas with the best blood supply. However, in solid tumors, sufficient blood supply is restricted to the periphery, and 90% of the

tumor receives little or no drug.[34] While this may result in an initial rapid reduction of the tumor volume, the death of only the outer cells often leads to continued inner growth and eventually an increase in tumor volume as cancer cells become resistant or tumor growth outpaces cell death.

Hypoxia (reduced oxygen partial pressure) further adds to the conundrum of solid tumors. Koong and colleagues were the first to measure the oxygenation of pancreatic tumors in humans. Examining seven different human patient samples, they found an extreme degree of hypoxia in pancreatic tumor tissue. The partial pressure of oxygen (pO_2) in these tumors ranged from 0 to 5.3 mm Hg, while a normal pancreas range is 9.3 to 92.7 mm Hg. Multiple tumors had greater than 90% of measurements show a pO_2 of less than 2.5 mm Hg, indicating significant levels of hypoxia.[35] Studies in glioblastoma, sarcomas, head and neck carcinomas, breast, cervix, and prostate cancers have shown similar results for solid tumors.[36–42] Cancer cells are able to adapt to this hostile environment through transcriptional activity of hypoxia-inducible factors (HIF1 and HIF2). Hypoxia, along with HIFs, play intricate roles in regulating the expression of multiple genes involved in glucose metabolism, angiogenesis, cell invasion, metastasis, and significantly increases risk of cancer mortality.[43,44,45–47]

The tumor's microenvironment plays a crucial role in pancreatic cancer. Composed of many cell types including: fibroblasts, adipocytes, endothelial cells, and others, its obvious cells within the tumor are not homogenous.[6–8] This heterogeneity leads to a unique environment with significant fibrosis (desmoplasia) and a dense extracellular matrix. Cancer stem cells (CSCs), sometimes referred to as tumor-initiating cells, within this microenvironment have been identified in a large number of human malignancies and possess the capacity to self-renew. While often representing less than 1% of cells present, the CSCs significantly contribute to chemotherapy resistance, metastasis, and relapse.[48,49,50] Hypoxia and the HIF proteins have been

shown to further induce self-renewal of these CSCs as well as inhibit their differentiation in multiple cancer types.[51–53]The preference of CSCs to accumulate in hypoxic niches makes targeting and eliminating these cells difficult as there is a lack of vasculature preventing chemotherapy from accessing these sites. The signal transducer and activator of transcription (STAT3) gene encodes a transcription factor pivotal in stem cell self-renewal. Persistent activation of STAT3 is observed in multiple gastrointestinal cancers including hepatocellular, pancreas, and colon carcinomas.[54–56] Evidence shows STAT3 interacts with CD44, upregulates NANOG, and induces CSC like properties in cancer cells.[57,58,59,60]

Pancreatic cancer cells are reported to overexpress the neuropilin-1 receptor.[61] We previously demonstrated that pancreatic CSCs also overexpress this receptor.[62] A small circular peptide known as iRGD, named for its specific amino acid sequence, has been previously reported as a cell penetrating peptide.[63] The iRGD, binds to $\alpha_V\beta_3$ and $\alpha_V\beta_5$ integrins on the cell surface.[64] Once bound, proteolytic enzymes cleave the iRGD peptide altering its specificity towards the neuropilin-1 receptor. Binding of the neuropillin-1 receptor induces two important pathways. First, downstream signaling allows endocytosis of the receptor by a macropinocytosis mechanism. The vacuoles produced by macropinocytosis range from 0.2 up to 3 μm in size.[65] The polymersome bound to the receptor is included into these vacuoles allowing entrance into the cell. The second mechanism, transcytosis, is initiated allowing increased tissue penetration and cargo delivery deep into the tumors.[63,66,67]The increased expression of these receptors on pancreatic cancer cells acts as an active targeting mechanism for our polymersomes. Any free drug released or leeched from the nanoparticles will still be able to enter the cell via their influx transporters. Gemcitabine mainly enters through the SLC29A1 and SLC28A3 transporters and efflux by multiple ABC transporters (ABCC3, 5, and 10).[68,69] Napabucasin, being a highly

lipophilic drug is able to readily enter cells via passive diffusion. Any influx/efflux transporters directly interacting with napabucasin have yet to be elucidated.

These hypoxia-induced changes to solid tumor cells, along with resilient CSCs, necessitate the need for deep-penetrating drug carriers that target the hypoxic niches of solid tumors. Herein, we report a tumor-penetrating, hypoxia-responsive, polymeric carrier (polymersome) composed of PEG and PLA, which releases encapsulated drugs in the reducing microenvironment of the hypoxic-niches inside solid pancreatic tumors. Previous use of these hypoxia responsive polymersomes in our laboratory using gemcitabine and an epidermal growth factor receptor inhibitor (erlotinib) showed increased response to treatment in spheroidal cultures of BxPC-3 pancreatic cancer cells.[70] Here, we encapsulated a top chemotherapy treatment option for pancreatic cancer, gemcitabine, along with a drug currently in clinical trials as a STAT3 inhibitor, napabucasin. Napabucasin has been shown to lower tumor self-renewal by CSC and induce apoptosis in this cellular subset in a variety of solid tumors.[71–74] Incorporating a drug with well-documented clinical efficacy in pancreatic cancer (gemcitabine) along with a STAT3 inhibitor, we hypothesized a greater effect on tumor suppression and prevention of tumor self-renewal from inside the tumor core.

Results and Discussion

Synthesis of hypoxia-responsive copolymers (PEG-AZO-PLA), tumor-penetrating peptide-polymer conjugate (PLA-PEG-iRGD), and tumor penetrating polymersome.

In our polymersome design, a 4,4'-diazobenzene is used for linking the hydrophilic polyethylene glycol (PEG 2K molecular weight) and the hydrophobic polylactic acid (PLA 7K molecular weight) of the diblock copolymer (Figure 2A). Biological reducing environments are amplified under hypoxic conditions.[75,76] The addition of this 4,4'-diazobenzene functional group that is

sensitive to this environment allows for the triggered delivery of the encapsulated payload.[70,77] Both polymer blocks are approved for human use by the US Food and Drug Administration (FDA), and are classified into the "generally regarded as safe" category. We synthesized the copolymer by ring opening polymerization of DL-lactide using Sn(octanoate)$_2$ as the catalyst. Hence, the resultant copolymer is racemic. Next we recrystallized commercially available DL-lactide and carefully controlled the reaction conditions to reduce the polydispersity of the resultant polymer. The resultant polymer is precipitated and removed via filtration to remove any residual Sn(octanoate)$_2$. The purified hypoxia-responsive polymer PEG$_{2000}$ –diazobenzene–PLA$_{6000}$ was characterized by ^{1}H and ^{13}C NMR spectroscopy and gel-permeation chromatography (GPC, Appendix, Figure A1-A3). Analysis of the GPC data showed a polydispersity index of 1.12 for the hypoxia-responsive copolymer.

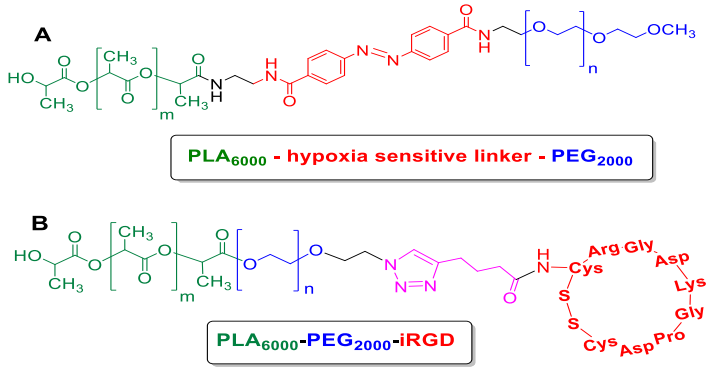

Figure 2. Polymersome Components. (A) diblock copolymer consisting of polyethylene glycol linked to poly lactic acid by the hypoxia-sensitive 4,4'-diazobenzene linker (red), and (B) iRGD peptide conjugated to the PLA-PEG copolymer.

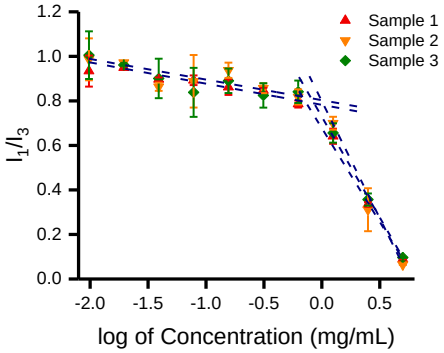

Figure 3. Critical Aggregation Concentration. Resulting value of 0.87 mg/mL ± 0.05.

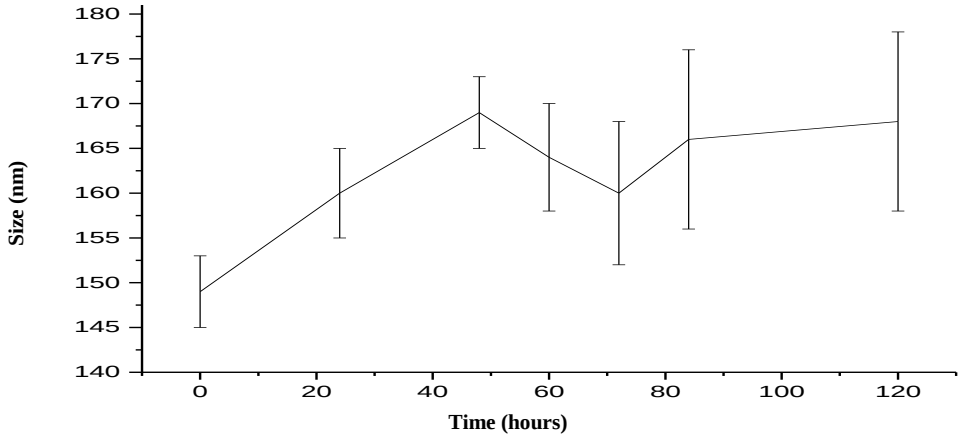

Figure 4. Polymersome Stability in Serum. The initial size was 149 (±4) nm and after 120 hours the average size was 168 (±) nm. n=3

The synthesis of the PLA-PEG-iRGD polymer (Figure 2B) was a two-step process. First, we synthesized N_3-PEG_{2000}-PLA_{6000} polymer following our previously reported protocol.[78] Protocol in brief, an azide PEG derivative reacts with D,L-lactide and dioctanoyl tin under reflux and precipitated in either. Next, we conjugated the synthesized hexynoic acid-iRGD to N_3-PEG_{2000}-PLA_{6000} using the Cu^{2+}-catalyzed Click chemistry ([2+3]-cycloaddition). Further r experimental details can be found in Materials and Methods. We determined the critical aggregation concentration of the synthesized hypoxia-responsive polymer to be 0.86 $\pm$ 0.051 mg/ml employing fluorescence spectroscopy of added pyrene (Figure 3).[79,80] We prepared the polymersomes from the hypoxia-responsive polymer (85%), the PLA-PEG-iRGD polymer (10%), and a fluorescent reporter, 1,2-dipalmitoyl-*sn*-glycero-3-phosphoethanolamine-N-lissamine-rhodamine B sulfonyl ammonium salt (5%), employing the reported solvent-exchange method.[81]

The effectiveness of a nanoparticle formulation can be dramatically changed by its characteristics.[82,83] We determined the size and shape of the polymersomes by transmission electron microscopy (TEM), atomic force microscopy (AFM), and dynamic light scattering (DLS) (Table 1). The enhanced permeability and retention effect, while being controversial, is

still widely considered to be a key factor in allowing the accumulation of nanoparticles in and around the tumor tissues.[84–86]Specifically, rapid angiogenesis induced by tumor cells, produces a structurally poor vasculature that allows for nanoparticles to extravasate and accumulate in and around the tumor. In addition to TEM and AFM (Figure 5A,B,C) images, the hydrodynamic diameter, polydispersity index, and zeta-potential of the polymersomes were determined by dynamic light scattering (Table 1). An average size of 107 (+/-2), 117 (+/-2), and 188 (+/-6) nm for control polymersomes (containing iRGD and HEPES buffer), iGem (gemcitabine encapsulated iRGD polymersomes), and iNap (napabucasin encapsulated iRGD polymersomes) respectively were measured. Gemcitabine is a hydrophilic drug and resides in the aqueous core of the polymersomes. However, napabucasin, being hydrophobic, partitions into the bilayer of the polymer vesicles, causing the increase in vesicle size. These polymersomes fit into a size window, where they are large enough to escape renal filtration (>10 nm), yet, small enough (<200 nm) to potentially avoid significant uptake by the mononuclear phagocyte system.[26,87–89]

The stability of the polymersomes was investigated by adding buffer loaded iRGD-polymersomes to serum isolated from mice. The polymersomes average size increased by about 20 nm within 48 hours of incubation with serum and they then maintained that average size for up to 120 hours (Figure 4). The increase in size is likely due to adhesion of molecules within the serum to the polymersomes. This phenomonon is referred to as the protein corona. Adherent proteins make removal by our immune system quicker and may also alter cell uptake.

Table 1. Polymersome Characterization

Sample Name:	Size (nm)	Poly Dispersity Index	Zeta-Potential
Control Polymersome	107 ± 2	0.11	-3.2 ± 0.4 mV
iGem	117 ± 2	0.14	-10.3 ± 0.5 mV
iNap	188 ± 6	0.3	0.1 ± 0.4 mV

The exact pharmacodynamics and pharmacokinetics of this formulation are outside the scope of this study and are reserved for future investigation. Preliminary studies showed no or minimal entrance into the CNS and blood brain barrier after 72 hours. These studies were conducted using a transwell assay with bEnd.3 brain endothelial cells. Additionally, we lack the facilities to complete radio-labeling in-vivo studies to accurately determine half-life of the encapsulated drugs.

Next, we demonstrated the polymersomes' ability to release the encapsulated contents under hypoxic conditions (2% oxygen). A fluorescent dye, carboxyfluorescein, was encapsulated into the polymersomes. We used human liver microsomes as an oxidizing enzyme of NADPH to NADP+. This reaction provides reducing electrons that will break the azobenzene containing polymersomes (Scheme 1).[90] A hypoxia chamber set to 2% oxygen was to further mimic hypoxic conditions (Figure 5D).[70] The release profile was monitored over time by measuring the fluorescence intensity of the solution. Our polymersome formulation was able to release 81% (± 3) of its contents under hypoxic conditions compared to only 21% (± 2) under normoxia after 60 minutes.

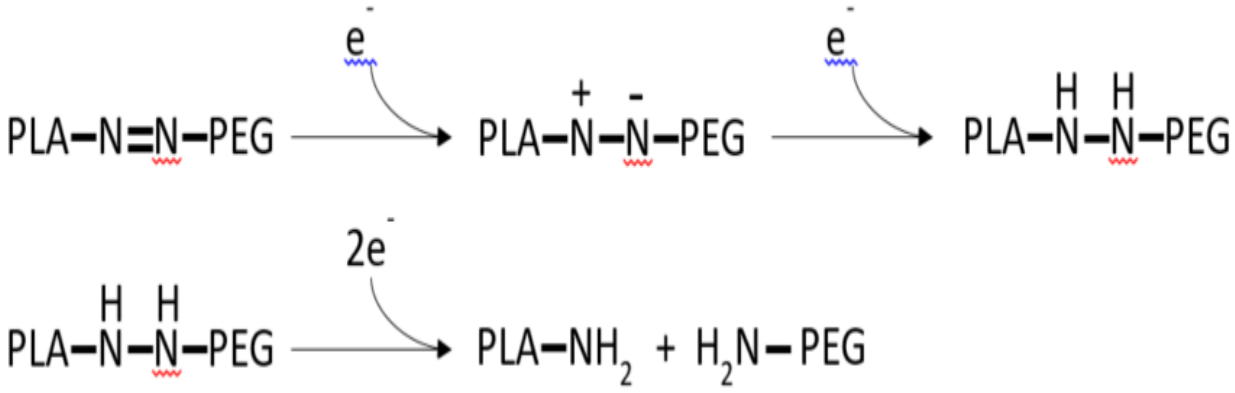

Scheme 1. Proposed Mechanism of Azobenzene Reduction

In-vitro cytotoxicity. Cytotoxicity was measured in a monolayer culture of BxPC-3 pancreatic cancer cells (Figure 6A). Previous studies demonstrated that hypoxia induces

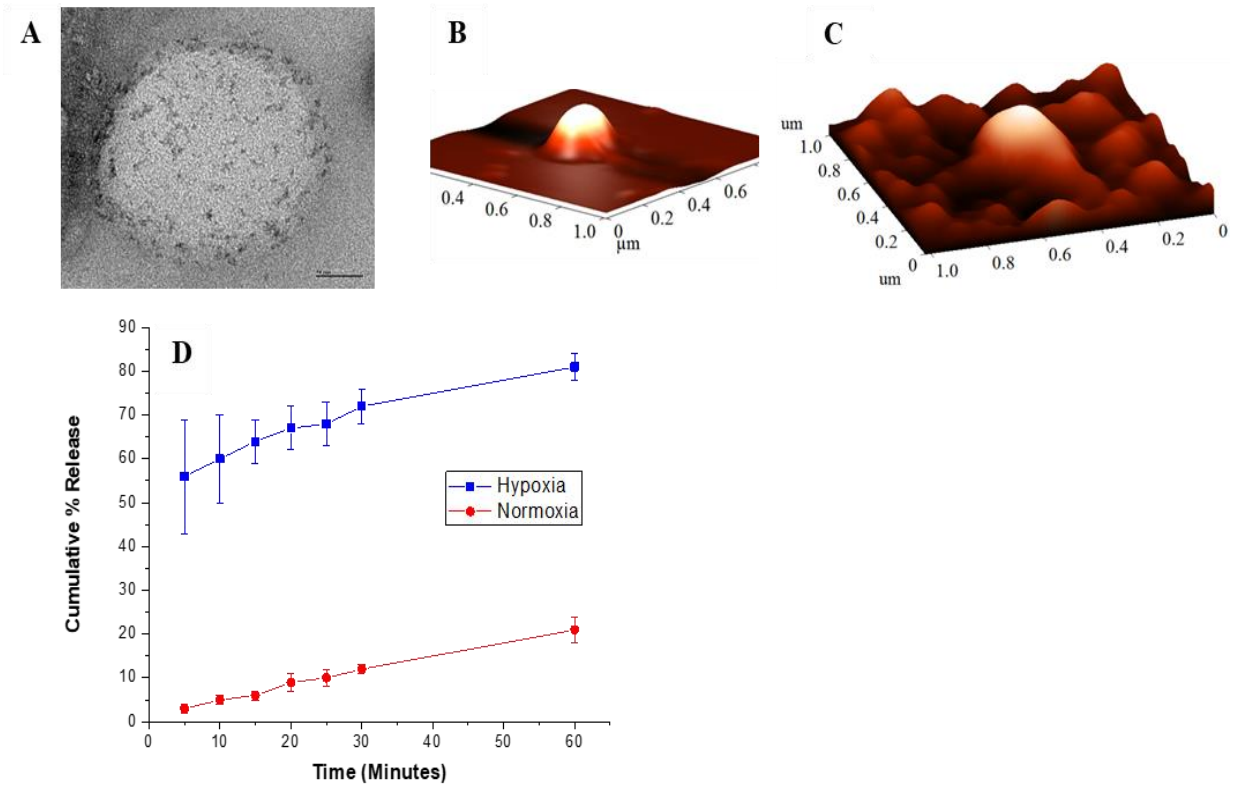

Figure 5. Characterization of Polymersomes. (A-C) Hypoxia-responsive iRGD peptide conjugated polymersomes' size and shape as shown by transmission electron microscopy (A) and atomic force microscopy under normoxic (A, B) and hypoxic conditions (C), respectively. (D) Carboxyfluorescein release under hypoxic and normoxic conditions with NADPH and liver microsomes.

biochemical and genetic changes in pancreatic cancer cells resulting in a more gemcitabine-resistant phenotype.[45,46,91–93] We observed that 73% (± 4) of cancer cells cultured in a hypoxic environment were viable after treatment with free gemcitabine compared to 48% (±3) viability after encapsulated (iGem) treatment. A similar result was observed with napbucasin that showed 74% (± 4) and 52% (± 3) viability between unencapsulated free drug and the encapsulated polymersome formulation respectively. iRGD polymersomes (iGem, iNap, and the drug combination iPsome) were able to either increase cellular toxicity or mitigate the resistant phenotype developed under hypoxia, possibly due to an increased uptake of the vesicles, resulting in higher drug concentrations inside the cells (Figure 6B). Next, we tested iRGD polymersomes using a three-dimensional (3D) model allowing gradients in oxygen, nutrients,

and metabolites, creating a more heterogeneous population along with physiological cell-cell interactions.[50, 51] Cell spheroids were prepared using 3D Petri Dish® from Microtissues®. We then tested free Gem and free Nap against the iRGD polymersomes encapsulating these drugs. A high chemoresistance (10-30% greater viability) under hypoxia was observed for the free drugs but was mitigated using the iRGD polymersomes (Figure 7A). A cell viability of 76% (± 4) and 71% (± 3) for unencapsulated free drugs gemcitabine and napabucasin, while the iRGD-polymersome formulations of these drugs were 60% (± 3) and 38% (± 4) respectively after 72

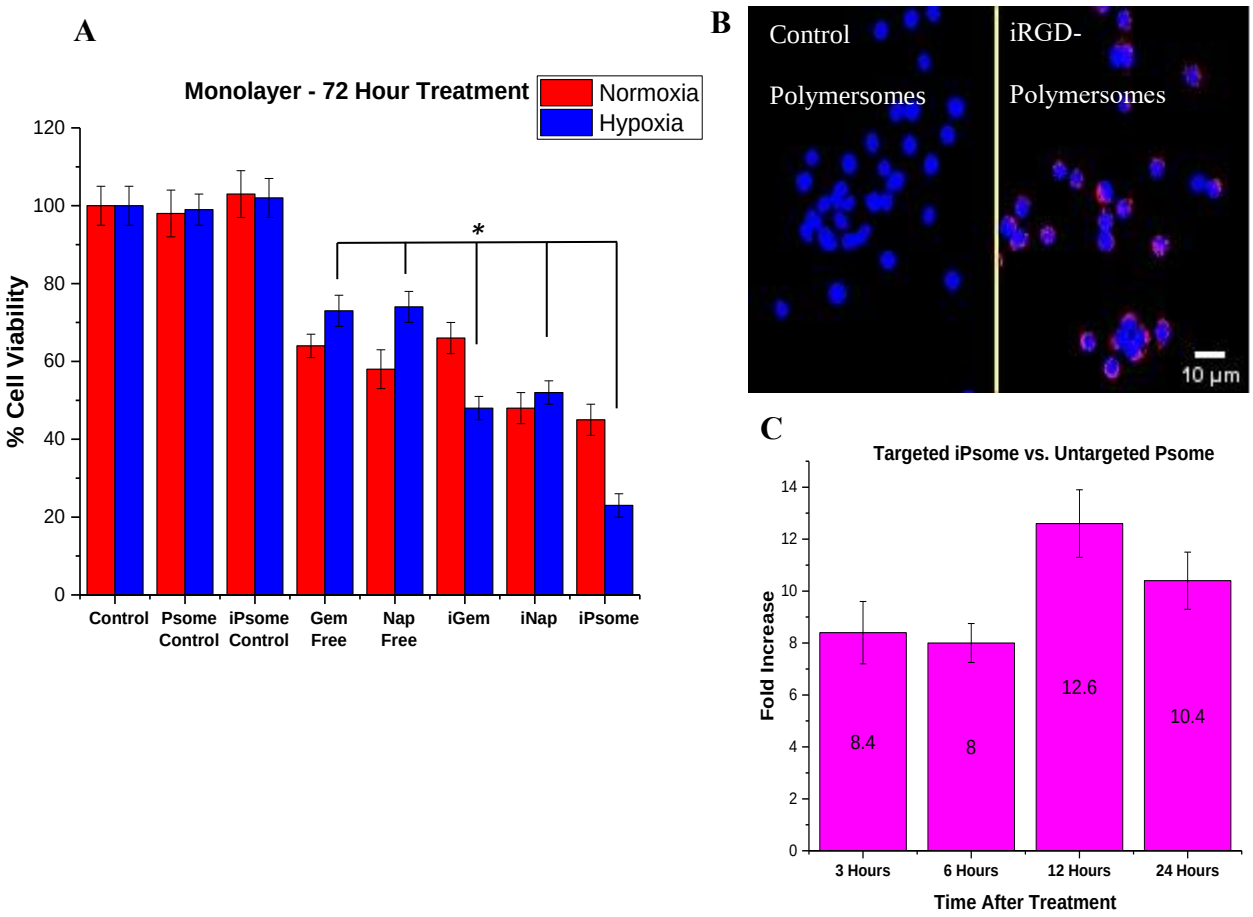

Figure 6. In-Vitro Monolayer Studies on Cell Viability. (A) Viability of BxPC-3 cells in monolayer cultures under normoxic and hypoxic (2% O_2) conditions. Control treatments lack encapsulated drugs. (B) Cellular uptake after 2 hours of iRGD conjugated hypoxia-responsive polymersomes in monolayer cultures of BxPC-3 cells. Control represents polymersomes without iRGD. (C) Cellular uptake using a FITC conjugated polymer and flow cytometry. Represents fold increase in cellular uptake at selected time points
***** p value <0.05, n = 8 (A), n=3 (C)

hours of treatment in hypoxic conditions. It is speculated that the polymersomes were better able to penetrate the dense spheroids as compared to the free drugs leading to overall decreased cell viability. This theory was previously examined by our lab, using an ex-vivo penetration apparatus that showed a penetration depth of 2.2mm.[77]

In-vitro uptake and internalization. The increased cellular toxicity of the drug-encapsulated polymersome formulations is likely due to a higher accumulation of the drugs in the cancer cells. To validate this hypothesis, uptake and internalization of fluorescently labeled polymersomes (incorporating a FITC-PEG-PLA polymer) into pancreatic cancer cells (BxPC-3) was studied using flow cytometry. The iRGD-targeted polymersomes showed 12-fold greater uptake after 12 hours of incubation with the BxPC-3 cells compared to the non-targeted

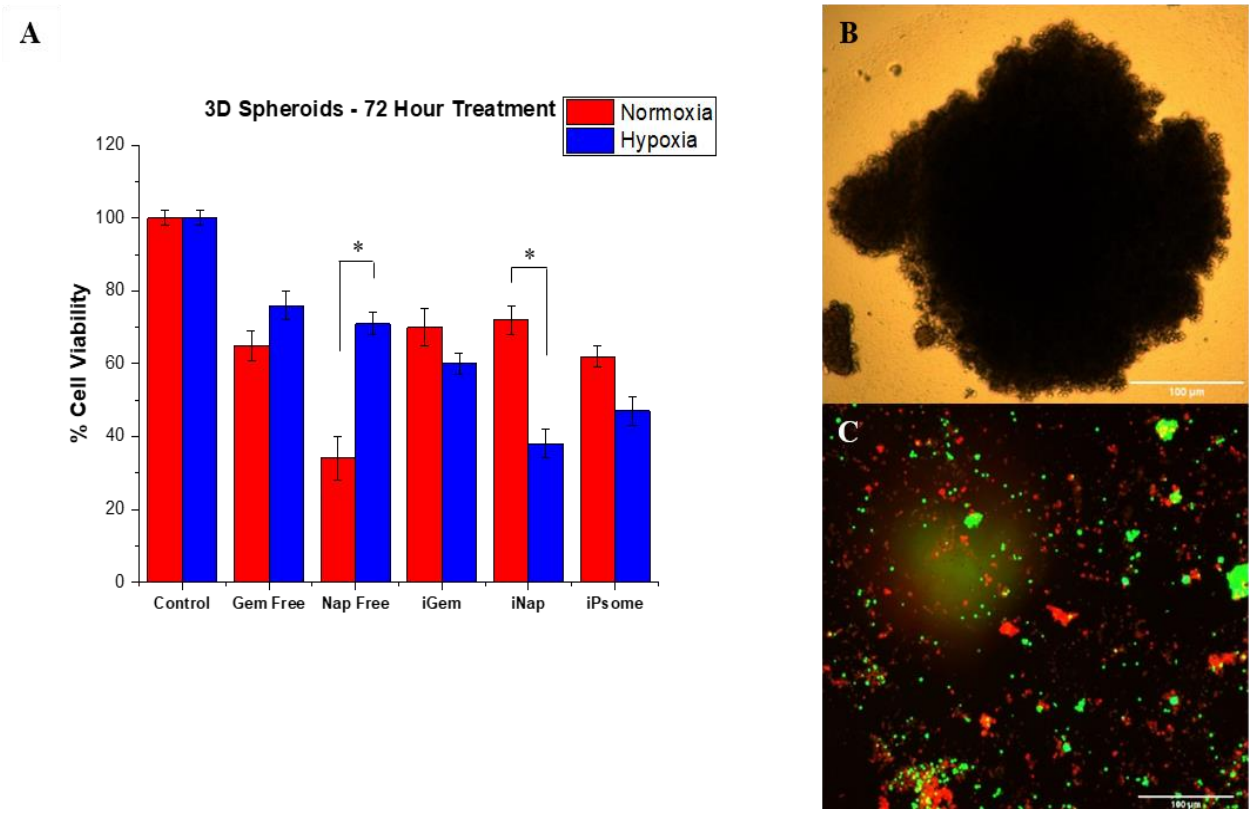

Figure 7. In-Vitro 3D Spheroids. (A) Viability of BxPC-3 cells in 3D spheroid cultures under normoxic and hypoxic (2% O_2) conditions. **(B)** Image of single spheroid pre-treatment. **(C)** Spheroid after 72 hour treatment with iRGD-polymersomes, using live (green) and dead (red) staining.
***** p value <0.05, n = 8

polymersomes lacking the iRGD (Figure 6C). A qualitative fluorescence microscopy experiment supported the significant difference in uptake of the iRGD-polymersomes in the pancreatic cancer cells compared to the non-targeted (no iRGD peptide) polymersomes after 6 hours of incubation (Figure 6B). The BxPC-3 cells are reported to overexpress the neuropilin receptor on the surface.[96,97] The enhanced uptake is likely due to the integrin and neuropilin-1 receptor targeting by the iRGD peptide.

Bio-distribution and accumulation of the polymersomes. One of the crucial properties for drug delivery vehicles is having a longer retention time in circulation. To evaluate the circulation time of the iRGD-polymersomes, we injected fluorescently labeled iRGD-polymersomes into non-tumor bearing NOD skid gamma (NSG) mice. These mice lack specific immune components and may portray a longer circulation time compared to normal mice. The iRGD-polymersomes encapsulating the near infrared dye indocyanine green (10 μM, excitation: 820 nm; emission 850 nm) suspended in 200 μL of phosphate buffered saline were injected in the mice though the tail vein.[98] Blood (100 μL) was drawn at various time points (1 h, 24 h, 72 h), and the fluorescence intensity of indocyanine green was measured at excitation 820 nm and emission 850 nm. A right shift in ex/em maximum was seen compared to unencapsulated ICG (780/810, respectively). We observed that 20% of the injected polymersomes ICG signal remained after 72 hours (Figure 8B). The PEG polymer on the exterior of the polymersomes provides the stealth needed to delay uptake of the iRGD-polymersomes by the mononuclear phagocyte system.[13] While we lack the ability for standard pharmacokinetic testing using clearance and volume of distribution, the circulation times we observed put these nanoparticles in the range of other FDA approved PEGylated nanoparticles with half-lives from 20 hours to 5 days[13,99–103]. Further studies are needed to confirm this data.

Next we monitored tumor accumulation, BxPC-3 tumor bearing mice were injected with iRGD-polymersomes formulation and live images were recorded. Images were acquired 2 hours after injecting (tail vein) either a control (saline), or iRGD-polymersomes (buffer only). Even when a mouse had two flank tumors, we observed a high accumulation of the polymersomes in both tumors (Figure 8A). The organs were also examined for accumulation of polymersomes at

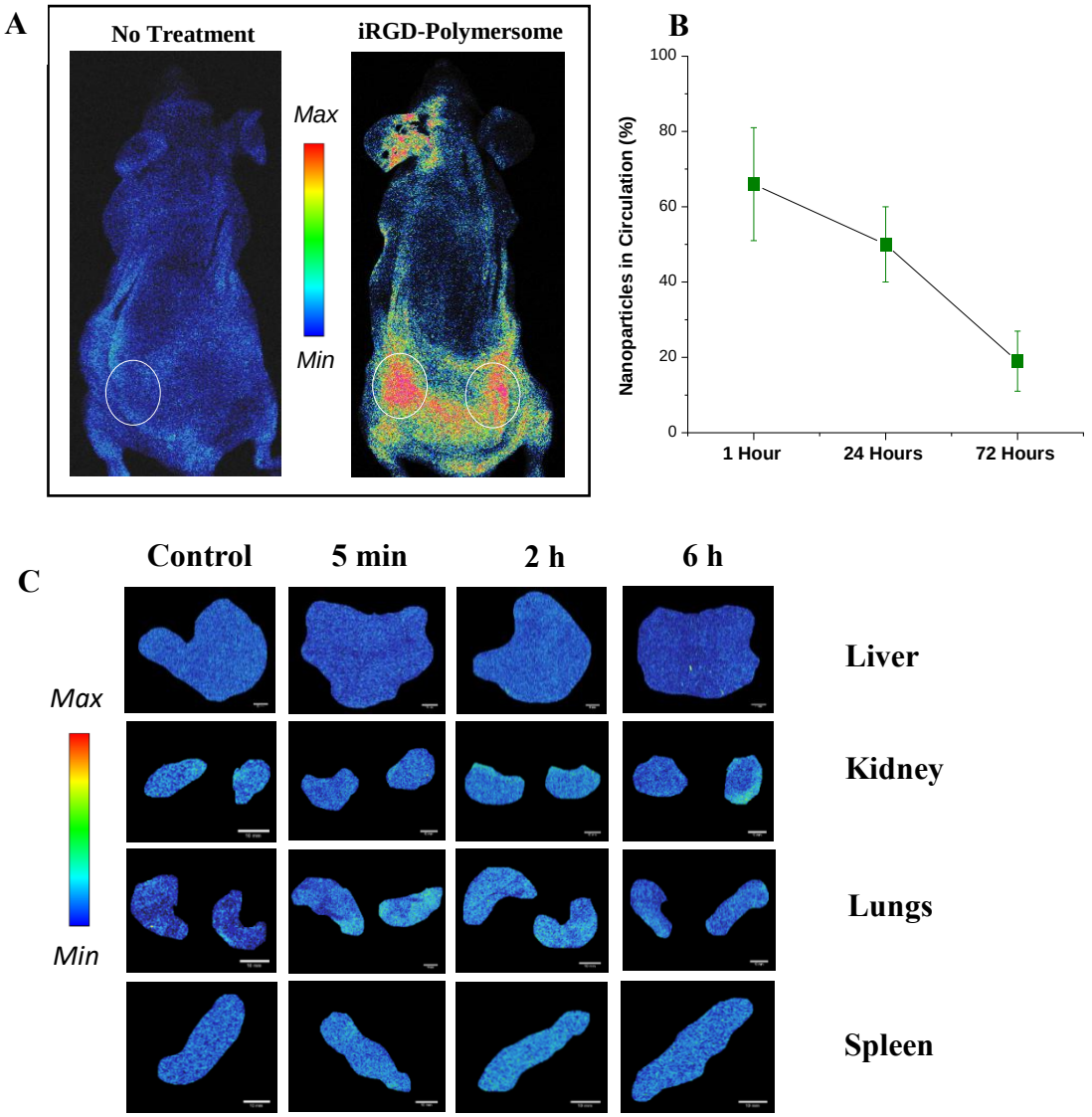

Figure 8. In-Vivo Bio-Distribution. (A) Mice with subcutaneous tumors (circled in white) injected with iRGD-polymersomes and imaged after two hours showing accumulation at tumor site. *Ear fluorescence from permanent marker used to label mouse. **(B)** Circulation time of iRGD-polymersomes based on remaining fluorescent signal in the blood. **(C)** Biodistribution to organs at 5 minutes, 2 hours, and 6 hours after tail vein injection of iRGD-polymersomes containing indocyanine green dye. (n = 3) (scale bar = 10mm)

various time points (Figure 8C). Some fluorescence signal was observed in the lung tissues. The accumulation of the polymersomes in the lungs is likely due to the presence of the neuropilin-1 (NRP-1) receptor on alveolar macrophages of the lung.[104] However, the accumulated polymersomes are unlikely to release excessive amounts of encapsulated drug in the lungs due to the high oxygen concentration. Quantification of polyermersome concentrations in these selected tissues has been reserved for future studies.

Hemoglobin and Oxygenation Saturation in a Mouse Model of PDAC. BxPC-3 (10^6) cells were injected into the pancreas of four athymic nude mice. Tumors grew to an average size of 500 mm^3, verified by ultrasound. Next, photoacoustic imaging was used to monitor tumor oxygenation. Hemoglobin oxygenation was determined by averaging three measurements from three different sites (normal pancreas, tumor edge, and tumor core). The average percentage of saturated oxygen (sO_2) was significantly different within these locations ($F_{(2,9)} = 7.85$, $p < 0.05$, Figures 9A). Specifically, sO_2 was significantly reduced in the tumor core, relative to both the tumor edge ($p < 0.05$) and normal adjacent pancreas ($p < 0.01$). Likewise, total hemoglobin (Figure 9B) was significantly different across locations ($F_{(2,9)} = 4.43$, $p < 0.05$) with the tumor core showing significantly less hemoglobin than the tumor edge and the normal adjacent

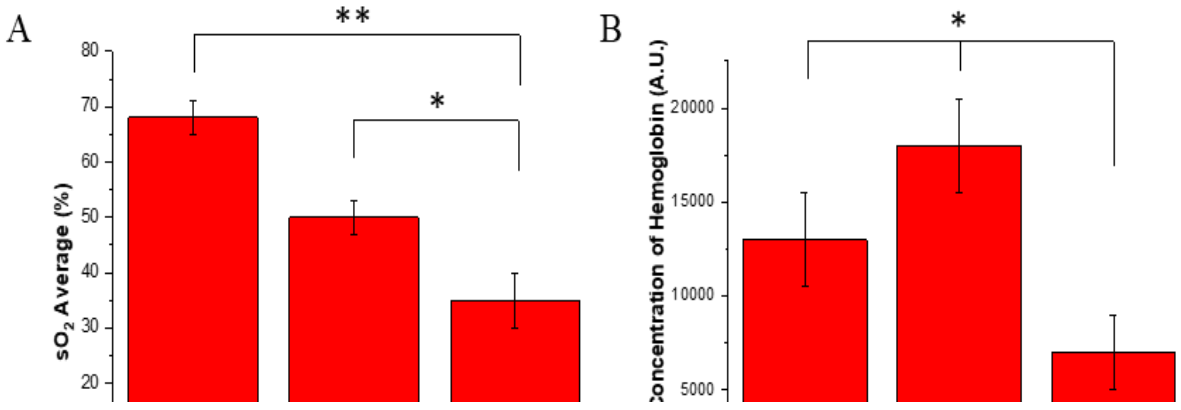

Figure 9. In-Vivo Saturated Oxygen and Hemoglobin. (A) Average saturated oxygen levels using PAI across all tumors. **(B)** Average concentration of hemoglobin across all tumors. * p value <0.05, ** p value <0.01, n = 4

pancreas ($p < 0.05$). Notably, these initial results resemble those seen in patient derived PDAC tumors.[35]The observed low levels of sO_2 indicates the presence of a hypoxic environment facilitating drug release from the polymersomes.

Tumor tissue staining for carbonic anhydrase IX and PECAM-1. A pilot study was conducted using excised tumor tissue to show a correlation between tumor hypoxia and poor vascularization. Carbonic anhydrase IX (CA IX) is transcriptionally regulated via HIF-1 and plays a significant role in acid-base regulation.[105]Due to its higher stability over HIF-1 it acts as an indirect measure of tissue hypoxia (Figure 10A.). Platelet endothelial cell adhesion molecule (PECAM-1) also known as CD31 is primarily used in immunohistochemistry to mark the

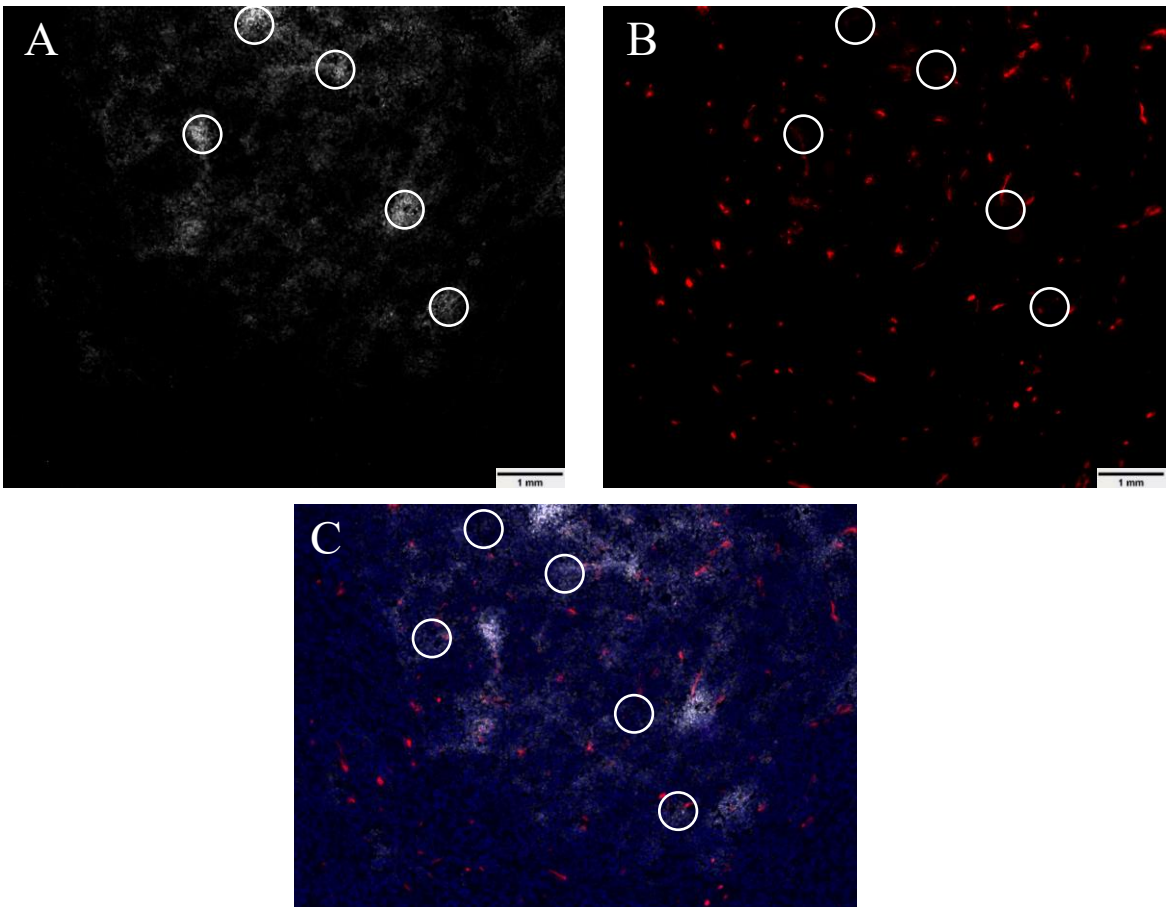

Figure 10. Immunohistochemistry of Excised Tumor Core. Excised tumors were sliced in half and the inner core was stained with CA IX (A), PECAM-1 (B), and a nucleus staining dye. The overlaid images can be seen in (C) indicating a lack of vasculature and angiogenesis. Scale bar represents 1 mm.

presence of endothelial cells and can help evaluate the degree of angiogenesis within the tumor (Figure 10B). We observed areas within the tumor core that had high levels of CA IX staining while simultaneously having low or no levels of PECAM-1 (Figure 10C). These findings further solidify the theory of hypoxic niches within the tumor.

Efficacy of polymersomes in subcutaneous mouse model of pancreatic cancer.

Athymic nude mice were injected with 10^6 BxPC-3 cells suspended in 200 µL of Matrigel® into the left flank and the tumors were allowed to grow for four weeks. Three male and three female mice were randomly assigned to each treatment group. Gemcitabine was dosed at 30 mg/kg and napabucasin was dosed at 20 mg/kg either as free drug or encapsulated into the polymersomes based on previously published animal data.[106,107] One week after the last treatment, we euthanized the mice and harvested the tumors. A significant decrease in tumor growth was observed for all drug encapsulated iRGD polymersome groups. The end stage tumor size was reduced by 242%, 254%, and 260% compared to no drug control for iGem, iNap, and the drug combination iPsome, respectively (Figure 12). A suppression of growth was also noted in the free drug groups of 113% and 118% reduced size for free gemcitabine and free napabucasin, but this was not significant compared to control. Interestingly, we observed that the drug encapsulated iRGD polymersome treatments rendered the tumors physically soft compared to the solid and dense control tumors. The resected tumors showed sunken fluid filled cores due to

Figure 11. In-Vivo Excised Tumors. Tumor outer surface (bottom) and tumor core (top).

vastly enhanced necrosis of the tumors from inside. In a few instances, the inside necrosis was so much that the overall tumor resembled a donut like structure. In general, the mice had no obvious treatment complications. Two mice from the two drug combination iPsome group were removed from the study after two weeks due to a decrease in body weight of greater than 15% as well as one mouse from the control and free gem group that were removed due to excessive tumor size affecting ambulation.

Histology Analysis. Tumors were collected at the conclusion of study (day 35), bisected, fixed, and embedded in paraffin wax. Tumor slices (10 µm thick) from the cut edge (tumor core) were placed on microscope slides, stained with hematoxylin and eosin, and analyzed using NIH ImageJ software. The area of necrosis was compared to the total area of tissue for that slide. The average area of necrosis was then compared between all treatment groups. The iRGD

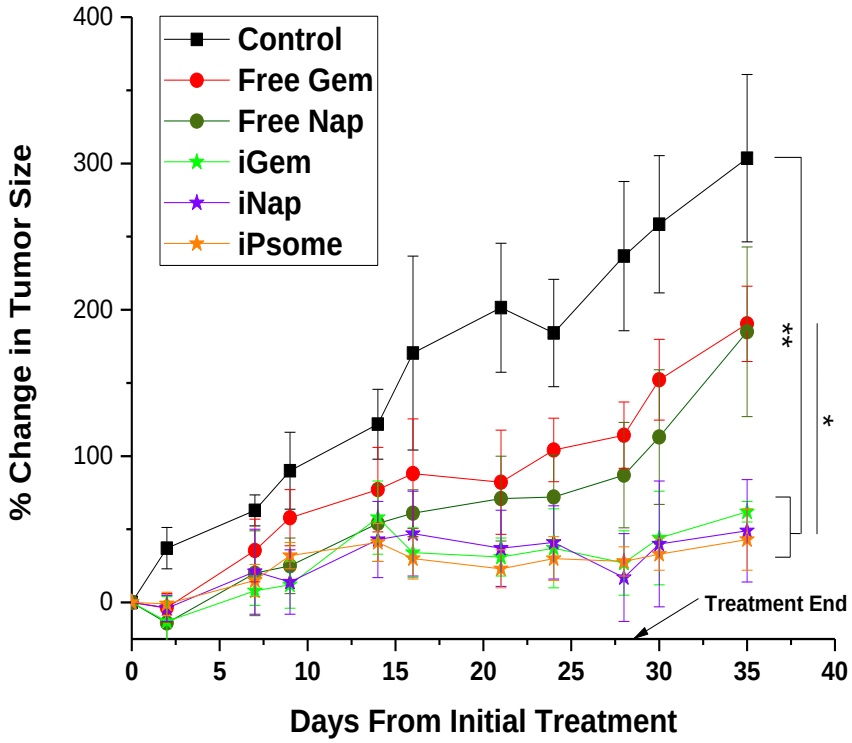

Figure 12. In-Vivo Animal Study. (**A)** Graphical representation of change in tumor size over the course of the treatment. Significant difference in the end stage tumor size between control and free drug groups vs. iRGD polymersome groups.
p value: * <0.05, ** <0.01
n = 5 (Free Nap, Free Gem, iGem, iNap) (Control = 4, iPsome = 4)

polymersome groups showed a significantly higher area of necrosis compared to saline treated controls and free drug groups (Figure 13B), with 25% more necrosis seen in iGem and iNap groups compared to free drug. Visually, the necrotic areas can be seen in the scanned slides with significant difference between free drug and the respective polymersome treatment group (Figure 13A).

Human Pancreatic Cancer Samples. To further assess the translational potential, we examined the tissue samples from two pancreatic cancer patients. Patient samples included a primary pancreatic tumor, unaffected pancreas tissue, and lung metastasis all from the same patient. We saw a 4-5 fold increased expression of both NRP-1 and STAT3 proteins in the primary tumor as well as the metastatic liver site (Figure 14). High expression of NRP-1 in PDAC is associated with other clinicopathologic characteristics such as lymph node involvement, advanced T stage, and decreased survival time.[108]Insinuating that the most lethal PDAC tumors may have high NRP-1 levels and better targets for our nanoparticle therapy.

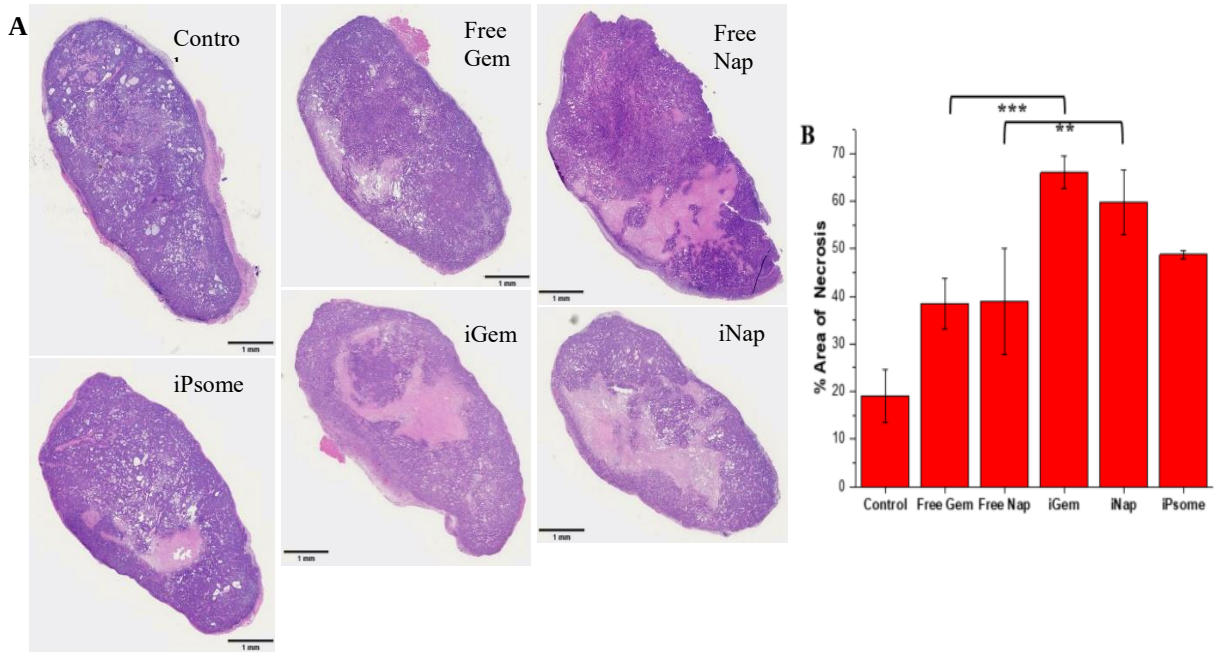

Figure 13. Excised Tumor Histology. (A) Excised tumors were sliced in half, formalin fixed, embedded in paraffin wax and stained using hematoxylin and eosin. (B) Calculated and averaged total necrotic area for each tissue section. **p value< 0.01 , ***p value <0.001

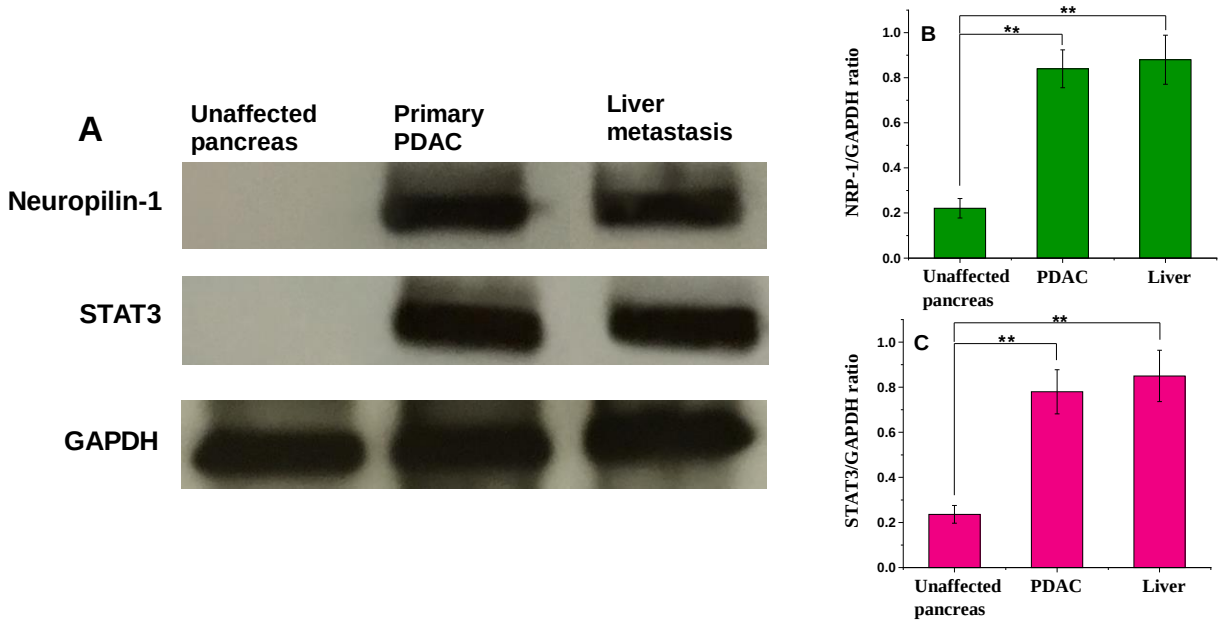

Figure 14. Western Blot of Human Pancreatic Cancer. (**A**) Western blot of the unaffected pancreas, primary pancreatic tumor, lung metastatic site, and liver metastatic site all from the same patient. (**B**) NRP-1 to GAPDH expression ratio. (**C**) STAT3 to GAPDH expression ratio. **p value< 0.01

Conclusion

Pancreatic cancer patients often have minimal clinical success. The 5-year survival rate has remained below 10% for over 40 years and only in the last 10 years have these rates been above 5%.[109] Potentially, targeting the hypoxic tumor core may pose a strategic advantage to these patients. Utilizing polymeric nanoparticles with a tumor penetrating iRGD peptide and a hypoxia-responsive system, we were able to increase cellular toxicity and uptake to cancer cells to combat hypoxia-induced resistance. These polymersomes were able to increase cellular toxicity by nearly 50% compared to unencapsulated drugs. The incorporation of the iRGD peptide allowed for a 12-fold increase in cellular uptake as compared to polymersomes lacking this peptide. These initial results compelled us to further investigate the therapeutic potential of an inside-out treatment strategy. Upon completion of our animal study using a mouse model of pancreatic cancer, we found intriguing results. First, the apparent tumor size and volume was decreased by over 200% compared to untreated controls. Interestingly, tumor volume bounced

back up immediately when the treatment had stopped in case of free drug group whereas the tumor volume stayed relatively steady when treated with iRGD polymersome encapsulated drugs. This result potentially suggests that iRGD polymersome encapsulated drugs decreased the number of free drug resistant cancer cells and delays cancer recurrence. Second, and possibly most alluring, were the resected tumors. The iRGD polymersome groups had tumors that were subjectively squishy, and fluid filled compared to either the free drug or control tumors. The final finding of increased necrosis in the tumor core, was another indication that our tumor penetrating polymersomes were effective in delivering their payload deep inside the tumor tissue.

Our future studies aim to better discern the possible toxicity associated with these nanoparticles and better understand pharmacokinetics of these small particles. The polymersomes were able to suppress tumor growth, but in the end the tumors did not achieve complete remission. An optimization of treatment protocol or a possible combination of these polymersomes with a non-penetrating chemotherapy may have a better chance at achieving complete remission.

Materials and Methods

Materials. The amino acids and resin beads for peptide synthesis were purchased from Peptides International. Polymers for synthesis of the diblock copolymer were purchased from Biochempeg. The fluorescent lipid 1,2-dipalmitoyl-*sn*-glycero-3-phosphoethanolamine-N-lissamine rhodamine B sulfonyl ammonium salt was purchased from Avanti Polar Lipids. Pancreatic cancer cell line (BxPC-3) was obtained from American Type Cell Culture, USA. The solutions used for cell culture including; media, fetal bovine serum, and 100X antibiotic solution was purchased from VWR International. The nude lab mice were purchased from Envigo labs.

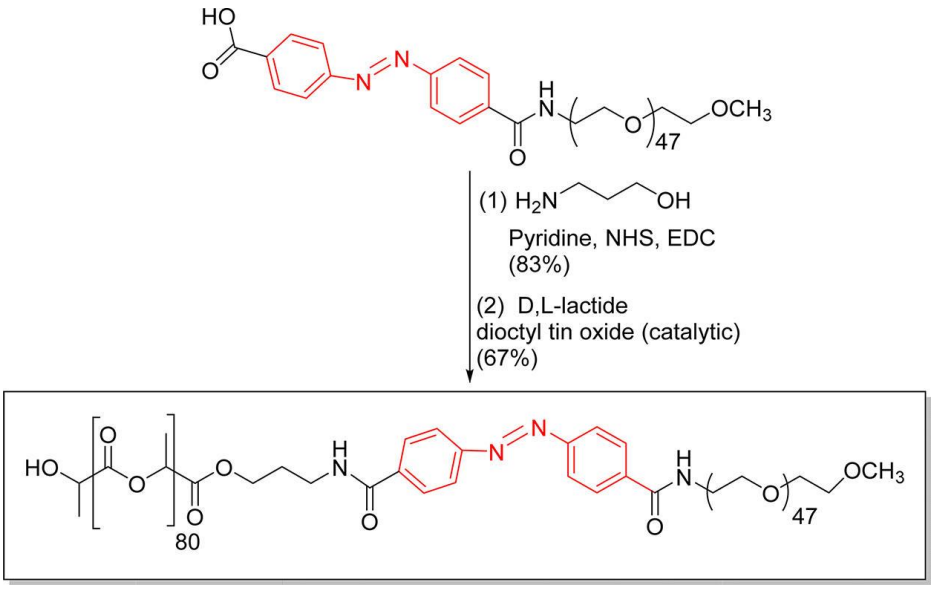

Scheme 2. Synthesis of Hypoxia-Responsive Copolymer

Synthesis and characterization of hypoxia responsive polymer PEG-azobenzene-PLA. Polymer m-PEG_{2000}−NH_2 was conjugated to azobenzene-4,4′-dicarboxylic acid by following a previously published protocol.[110] The PEG−diphenylazacarboxylate (50 mg, 0.023 mmol) was dissolved in pyridine (1.25 mL). To this solution, 1-ethyl-3-(3-dimethylaminopropyl)-carbodiimide (EDC.HCl; 6.7 mg, 0.0345 mmol) and N-hydroxysuccinimide (NHS; 4 mg, 0.0345 mmol) were added followed by excess 3-aminopropanol (8.75 mg, 0.116 mmol). The reaction mixture was stirred at room temperature overnight. The solvent was then evaporated under reduced pressure. The residue obtained was dissolved in dichloromethane (10 mL) and washed with water three times, the bottom organic layer was dried under vacuum, yielding 34 mg (67%) of yellow solid product. ^{1}H NMR (400 MHz, chloroform-d) δ ppm: 8.00-8.23(CH=CH- CH, m, 8 H), 3.67 ((CH_2-CH_2-O), t, 4 H), 3.40 ((CH_3-O), s, 3 H), 0.88 ((NH-CH_2-CH_2- CH_2-OH), m, 2 H).

Synthesis of the block copolymer. The product obtained from the previous step (100 mg, 0.05 mmol), D,L-lactide (500 mg, 3.5mmol) and tin(II) ethoxyhexanoate (3 □L, 0.009 mmol) were added to anhydrous toluene (5 mL) in a 35 mL glass high pressure vessel, then filled

with nitrogen. The solution was stirred at 120° C under nitrogen for 24 hours. After cooling to room temperature, the reaction mixture was added dropwise to cold ether. The top clear supernatant was decanted, and the precipitate was washed again with ether, dried under vacuum. The orange solid product obtained (305 mg, 51%) was analyzed by ^{1}H NMR spectroscopy and gel permeation chromatography. ^{1}H NMR (400 MHz, chloroform-d) δ ppm: 5.19 ((-CH-C=O), q, 1 H), 3.67 ((CH_2-CH_2-O), t, 4 H), 1.59 ((CH_3-CH-C=O), d, 3 H) (Appendix, A1-A3).

Determination of copolymer composition. The repeating monomer number m of PLA was also estimated from ^{1}H NMR by comparing (-CH-C=O) (δ ppm = 5.19 from the PLA block) to $-(OCH_2CH_2)_n-$ (δ ppm = 3.67 from the PEG block), m is the number of protons of -CH-C=O; 4n is the number of protons of $-(OCH_2CH_2)_n-$

$m/4n = a_1/a_2$: a_1 = area of peak at 5.19 ppm a_2 = area of peak at 3.67 ppm

Mw of PEG = 2000, n = 46, 4n = 184, then $m = 188a_1/a_2$, then Mw (PLA) = 5900

Synthesis and characterization of the iRGD peptide. Microwave-assisted, solid phase peptide synthesis was carried out using a Liberty Blue (CEM Corporation). The resin used was a Rink amide (Protide purchased from CEM Corporation). The sequence hexynoic acid-Cys(Acm)-Arg(Pbf)-Gly-Asp(OBtu)-Lys(Boc)-Gly-Pro-Asp(OBtu)-Cys(Acm)-OH was synthesized without the final deprotection step. To cyclize, 0.1 mmol thallium trifluoroacetate in DMF (5 mL) was stirred with the peptide-resin conjugate for 1 hour. The resin was then washed with DMF and dichloromethane 3 times. Next, the peptide was cleaved from the resin using trifluoroacetic acid (19 mL), distilled water, (0.5 mL), and triisopropylsilane (0.5 mL) for 2 hours. Whatman Grade 1 qualitative filter paper was used to collect the peptide in a 50 mL centrifuge tube to which 30 mL of ice cold diethyl ether was added. The precipitate was collected and dried in a vacuum desiccator overnight. The dried product was then characterized

by MALDI-TOF mass spectrometry (observed mass: 1041.42, expected mass: 1042.43, elemental composition $C_{41}H_{64}N_{14}O_{14}S_2$, Appendix, Figure A4)

Synthesis of iRGD peptide – polymer conjugate. The polymer PLA-PEG-N_3 was reacted with the alkyne (hexynoic acid) moiety of the iRGD peptide using Click chemistry (1:2 molar ratio peptide to polymer). The copper complex was made by mixing copper (II) sulfate with N,N,N',N',N"–penthamethyl diethylenetriamine (PMDETA) for 2 hours. Ascorbic acid solution (1.4 µmol) was prepared in distilled water. The reaction mixture was then stirred for 24 hours at room temperature. The stirred solution was then transferred to a 1000 kD dialysis bag and dialyzed against water for 72 hours to remove the catalyst (PMDETA and ascorbic acid) as well as unreacted iRGD peptide. The product was then analyzed by CD spectroscopy and FT-IR (Appendix, Figure A5).

Preparation of polymersomes. PEG-azobenzene-PLA and iRGD polymer conjugate was dissolved (10 mg/mL) in acetone, and lissamine rhodamine lipid (0.01 mg/mL) in chloroform. First, the lissamine rhodamine lipid was added to a clean glass vial and air dried. Next, polymers were added dropwise in a 85:10:5 ratio of PEG-azobenzene-PLA, iRGD-PEG-PLA, and lissamine respectively to HEPES buffer (10 mM and pH 7.4). The resulting mixture was stirred for 1 hour, bubbled air for 45 minutes (to evaporate acetone), and then sonicated in a water bath sonicator (VWR Symphony ultrasonic cleaner, Model: 97043-936) for 1 hour at 35 KHz. The polymersomes were then passed through a Sephadex G100 size exclusion column. The eluted polymersomes were collected and used for the studies. Encapsulation of drugs was achieved by passive or active loading. For passive loading, napabucasin was added to the polymer mixture and added to the HEPES buffer. For active loading, we utilized a citrate buffer (100 mM and pH 4) instead of HEPES. Once collected through the size exclusion column,

gemcitabine was added, then pH was adjusted to 8 by adding a 1 M sodium bicarbonate solution dropwise and testing the pH. This mixture was than stirred for 8 hours before passing through the size exclusion column again to remove unencapsulated drug.

Determination of critical aggregation concentration. From a stock solution of 0.1 mM pyrene in dichloromethane, 10 μL aliquots were taken in different vials, and the dichloromethane was allowed to evaporate in air. To each of these vials, various measured amounts of the polymer were added (stock solution concentration 10 mg/mL in a 1:5 acetone: deionized water solution by volume) so that the concentrations varied from 5 mg/mL to 9.8 □g/mL, and the final concentration of pyrene in each vial was 1 μM. The vials were sonicated at 35 KHz using a VWR Symphony ultrasonic cleaner (Model: 97043-936) for 45 minutes and then allowed to stand for 2 hours before recording the fluorescence spectra. The fluorescence emission spectra were recorded at an excitation wavelength of 337 nm with a bandwidth of 2.5 nm (for both excitation and emission). The ratio of the intensities at 373 nm and 393 nm were plotted against the concentration of the polymer, and the inflection point of the curve was used to determine the critical aggregation concentration.[79,80]

Size analysis of the polymersomes. The hydrodynamic diameter of the polymersomes was measured using dynamic light scattering, using a Malvern Zetasizer instrument and Zetasizer software version 7.02. One mL of sample was placed in a Sarstedt Cuvette. Sample was give 120 second equilibration time followed by three measurements each with ten runs. Atomic force microscopy was carried out in noncontact mode at a scanning rate of 0.7 Hz and a resonance frequency of 145 kHz using a NT-MDT NTEGRA (NT-MDT America). The cantilever was made of silicon nitride and was 100 μm long. Scanning area was 5 x 5 or 20 x 20 μm^2 at a resolution of 512 or 1024 points per line respectively. For electron microscopic

imaging, copper TEM grids (300-mesh, Formvar-carbon coated, Electron Microscopy Sciences) were prepared by applying a drop of 0.01% poly(L-lysine), allowing it to stand for 30 s, wicking off the liquid with torn filter paper, and allowing the grids to air-dry. A drop of the suspension diluted 1:100 was placed on a prepared grid for 30 s and wicked off; grids were allowed to air-dry again. Phosphotungstic acid, 0.1% pH adjusted to 7–8, was dropped onto the grid containing the sample, allowed to stand for 2 min, and wicked off. After the grids had dried, images were obtained using a JEOL JEM-2100 LaB6 transmission electron microscope (JEOL USA, Peabody, Massachusetts) running at 200 keV.

In-vitro uptake and internalization. Polymersomes were prepared using our standard protocol but in place of lissamine rhodamine B lipid, a FITC-PEG-PLA polymer was used at 5% concentration. Uptake was analyzed using an Accuri C6 flow cytometer with subsequent data analysis using FlowJo software (FlowJo, LLC).

Cell viability studies in monolayer culture. 5,000 BxPC-3 cells were seeded in each well of 96-well clear bottom plate. The cells were allowed 24 hours for attachment before placing in either a normal oxygen incubator (20% oxygen) or a hypoxia chamber (2% oxygen). The cells then grew for 24 hours before being subjected to their respective treatments. After 3 days, the media was removed, and cells were washed three times to remove any remaining polymersomes or drug. Subsequently, 20 µL of Alamar Blue (Invitrogen), a cell health indicator that uses the reducing power of living cells to quantitatively measure viability and 180 µL of fresh medium was added. The fluorescence was then measured, and viability was calculated.

Cell viability study in spheroid cultures. Spheroid scaffolds were prepared by adding agarose to a silicone mold (Microtissues) following the manufacturer's protocol using 96,000 cells/75 µL to produce a spheroid diameter of 200 µm. The seeded scaffolds were incubated for

7 days, changing the standard cell culture media every 2 days. The scaffolds were then placed in either normoxic (20%) or hypoxic (2%) conditions for 24 hours before being exposed to their respective treatments for 72 hours. After treatment, the scaffolds were washed with phosphate buffered saline before viability was analyzed by Celltiter-Glo 3D cell viability assay (Promega).

Orthotopic tumor implantation. Mice were first anesthetized by isoflurane (3% in 1 L/min 100% oxygen for induction and 2% in 1 L/min oxygen for maintenance). A cell suspension of 10^6 BxPC-3 cells in 25 µL sterile saline was injected into the pancreas using a 28G needle. The peritoneum was sutured back together using Ethicon Chromic Gut dissolvable sutures. The skin was then sutured with an Ethicon nylon suture. A topical antibiotic and tissue glue was used over the wound to prevent infection and help close the wound. The mice then received buprenorphine subcutaneous injection in the scruff of the neck for post-surgical pain. Mice were given welfare checks daily post-surgery.

Ultrasound and photoacoustic imaging of tumor volume and oxygenation. A VevoLAZR system equipped with LZ250 linear array transducer (VISUALSONICS) was used to measure tumor size and tumor oxygenation status (oxygenated/deoxygenated hemoglobin) A tunable laser with a pulse repetition rate of 10 Hz was used to excite the sample from 680-970 nm. Images were obtained under identical conditions using Vevo's 3D ultrasound imaging (B-mode) and Photoacoustics (PA) modes, respectively. Subsequent PA measurements of oxygenated/deoxygenated hemoglobin (750/850 nm absorption, respectively) were obtained in triplicate from the tumor core, edge and associated normal adjacent pancreas and subsequently quantified using Vevo's OxyZated analysis software.

In-vivo biodistribution. Athymic nude mice were used to establish subcutaneous tumors. Tumor bearing mice were injected with iRGD containing polymersomes and imaged

using a Kodak In-Vivo Multispectral Imaging System FX after two hours. Organ images were taken from mice lacking subcutaneous tumors. The mice were injected with the iRGD polymersome formulation via tail vein and were then euthanized at their respective time points (5 minutes, 2 hours, and 6 hours) and imaged using the Kodak camera at excitation 590 and emission 615.

In-vivo circulation time. iRGD polymersomes encapsulated with 12 µM ICG were injected (200 µL) via tail vein into 3 nude athymic mice. Blood draws (200 µL) were taken at 1 hour, 24 hours, and 72 hours post injection. The fluorescence was measured at excitation 820 and emission 850. The total remaining ICG was estimated by extrapolating the signal from 200 µL of blood to the total blood volume of the mouse using the equation total blood volume = 58.5 mL/kg.[111] A standard curve was made using various amounts of ICG and percent remaining was calculated use the initial 200 µL injection as a reference signal.[98]

In-vivo animal study. Six-week old nude athymic mice were purchased from Envigo Labs. BxPC-3 cells (1.5×10^6) were cultured, trypsonized, and re-suspended in Matrigel. The cell-Matrigel mixture was then injected into the right flank of the mice. Once tumors had reached a significant size (greater than 30 mm^3) as measured by calipers, the 36 mice were randomly allocated to each of the six treatment groups with three male and three females within each group. The control group received 200 µL of sterile saline, while the drug treatment groups received gemcitabine at 30 mg/kg and/or napabucasin at 20 mg/kg. Injections were given via tail vein using a 26G needle, twice weekly for four weeks. Mice were weighed and tumor volume measured using calipers before each injection. One week of observation continued after the treatment ended and tumor volume and weight were again measured twice during this time. Post observation period, the mice were euthanized via CO_2 followed by cervical dislocation.

Measurement by caliper. Estimated tumor volume was done using an external caliper. The greatest length and greatest width were selected and measured. The total tumor volume was calculated by the modified ellipsoidal formula.[112,113]

$$\textit{Tumor volume} = \tfrac{1}{2}(\textit{length} \times \textit{width}^2)$$

Animals. All mice were housed under standard housing conditions at the animal Core facility of NDSU, and all animal procedures were reviewed and approved by the Institute of Animal Care and Use Committee at the NDSU.

Acknowledgements

This research was supported by NIH grant 1 R01GM 114080 to SM. SM also acknowledges support from the Grand Challenge Initiative and the Office of the Dean, College of Health Profession, North Dakota State University. The animal core facility for housing and procedural supplies. The NDSU advanced imaging and microscopy lab for tissue processing and histology preparation.

HISTONE DEACTYLASE (HDAC) ENZYMES AS A RELEASE MECHANISM FOR ACETYLATED POLYMERSOMES

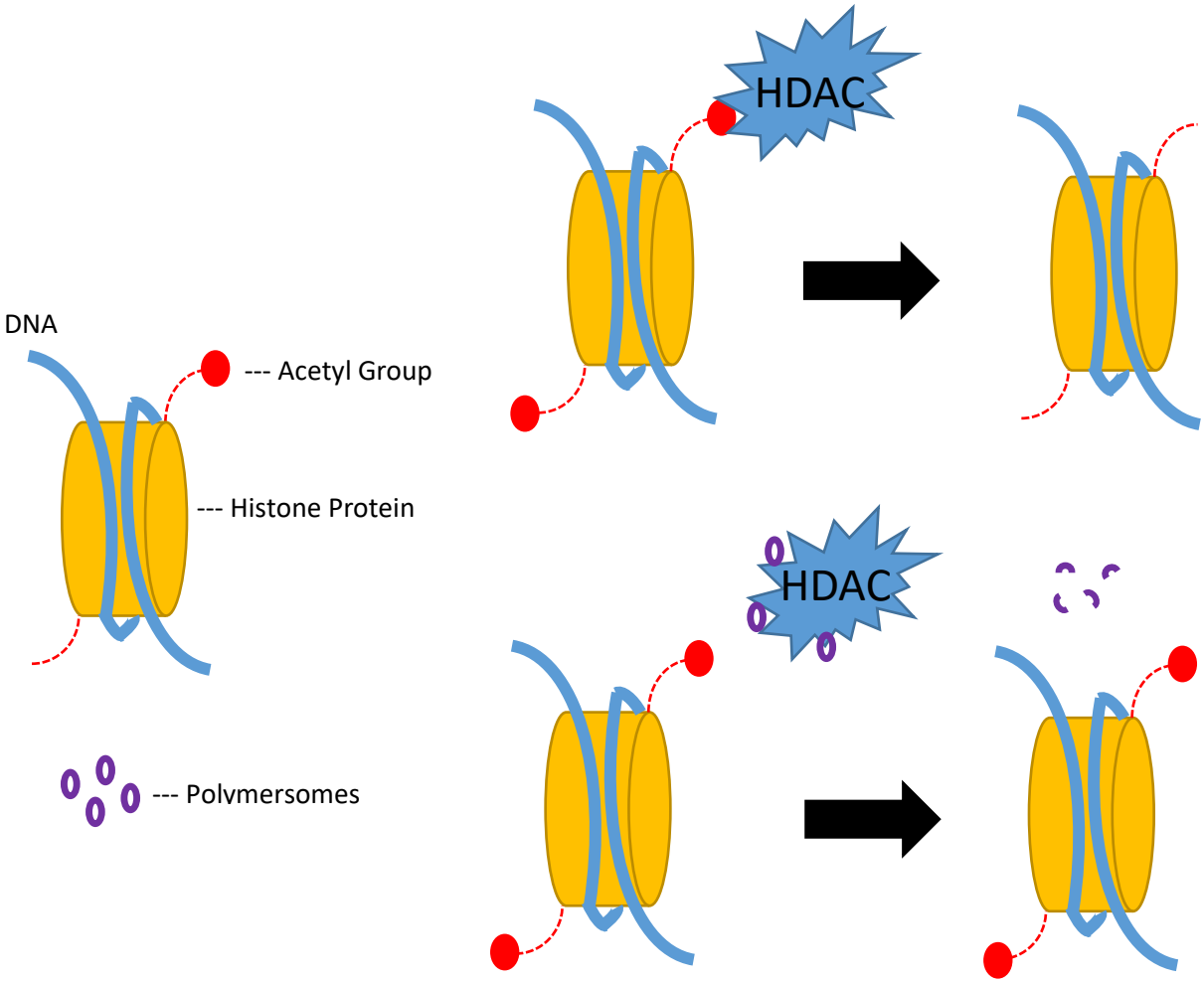

Figure 15. HDAC Nanoparticles Illustration

Abstract

Multiple drugs have recently been developed for inhibiting histone deactylase (HDAC) enzymes and preventing or altering their role in gene transcription. Altered expression of genes encoding HDACs has been linked to tumor development by induced transcription of genes that affect cellular functions. Specifically, functions relating to cell proliferation and apoptosis are of key importance. Unfortunately, these inhibitors have had little efficacy in solid tumors due to

many potential biological factors. An alternative strategy for modulating the function of HDACs, is to provide an excess of substrate to prevent the enzyme from performing its enzymatic deacetylation on target genes and/or the formation of corepressor complexes that often occur in the absence of a ligand. In this work, we created an acetylated block copolymer comprised of polyethylene glycol and a polylysine block. Acetylation of these lysine residues allows for self-assembled nanoparticles with an average diameter of 108 nm and a stability of up to 4 weeks. After incubation with HDAC enzymes, the nanoparticles lose their structure and collapse due to loss of hydrophobicity of the polylysine block, causing rapid release of encapsulated cargo. Cellular studies carried out on pancreatic cancer cells and stem cells using a STAT3 inhibitor (napabucasin) showed a 10 fold increased in potency and significant cytotoxicity to pancreatic stem cells in just 24 hours of treatment.

Introduction

Pancreatic cancer has an estimated 57,000 new cases in 2019 and 46,000 deaths.[114]Making up only 3% of all cancer diagnosis in the U.S., it accounts for 7% of all cancer deaths.[114] Mortality rates have incrementally increased (2007-2016 by 0.3%/year) leading us to believe current treatments are not effective. The most common treatments are gemcitabine based therapies, or a four drug combination chemotherapy cocktail, FOLFIRINOX (leucovorin, fluorouacil, irinotecan, and oxaliplatin), being used in select patients. These have modest benefits, but due to the resistance of cancer to gemcitabine as well as its off target toxicity, increased overall survival is limited.[115] A number of studies have been carried out to better understand the irregular gene expression and the alteration in the chromatin structures of the disease.[116] Of these gene expressions, some, very strongly indicate the pivotal role of histone deactylases (HDACs) for inducing transcriptional repression through chromatin condensation.

The progression of carcinogenesis has been attributed to the anomalous acetylation of histone tails.[117] Histone deacetylases are a class of enzymes that control critical cell functions by regulating the acetylation states of histone proteins and other non-histone protein targets.[118]It also plays a vital role in cancer initiation and progression.[119,120] In healthy cells, histone acetylation is precisely controlled by histone acetyl transferase (HAT) and HDAC but hyper-acetylation of oncogenes or hypo-acetylation of tumor suppressor genes is often seen in carcinogenic cells.[121,122] Histone acetylation and deacetylation processes are controlled by histone acetyltransferases (HATs) and histone deacetylatransferases (HDACs).[123] Lately, HDAC inhibitors have become largely popular as anti-cancer treatment drugs.[116,122] HDAC inhibitors disrupt the cell cycle and induce apoptosis. They interact with the catalytic site of HDACs, block substrate access and promote hyper acetylation of histone terminals.[116]

18 different HDAC isozymes have been identified in humans, and these are grouped, into four major classes. These classes are; class I (HDAC1, 2, 3, and 8), class II (HDAC4–7, 9, and 10), class III HDACs (sirtuins), and class IV (HDAC11).[124–126] It has also been reported that class I HDACs appear to be expressed only in the nucleus, while class II HDACs are found both in the cytoplasm and the nucleus.[127] Among all of the HDAC isozymes, HDAC8 has been reported to regulate the expression of tumor suppressor protein p53 in a HoxA-dependent manner[128–130] and has drawn a lot of attention as a target for several diseases including multiple types of cancer.[124,131] HDAC-8 and other HDAC enzymes in the class I category have been reported to bind to numerous transcription factors via nuclear-hormone corepressors NCOR (nuclear-receptor corepressor) and SMRT (silencing mediator for retinoid and thyroid-hormone receptors). Post binding to the strands of the chromatin, these enzymes operate via the mechanism of deacetylation of the histone tails and induce transcriptional repression.[129,132] This

repression, prevents the eventual production of various proteins and enzymes that regulate a plethora of cellular processes including: cell cycle, apoptosis, stress response, and DNA repair.

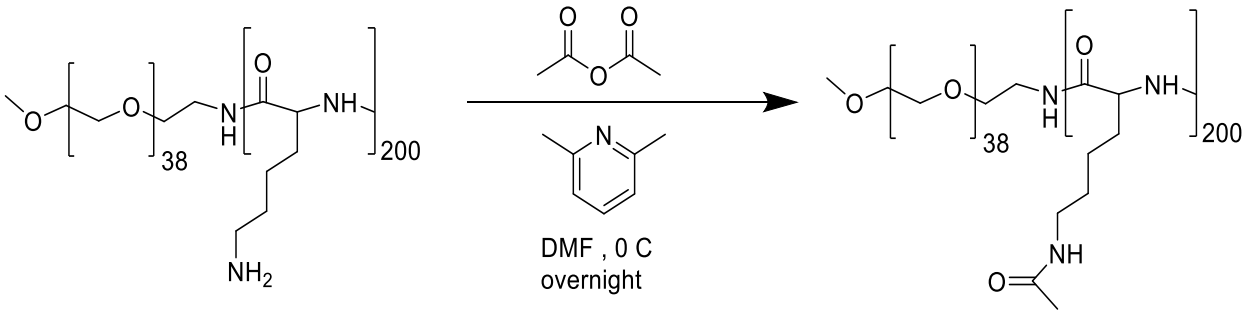

Scheme 3. Acetylation of Polylysine Block

A number of HDAC inhibitors have become popular as anti-cancer therapeutic agents and several studies have also shown these inhibitors to be active in vivo and in vitro for pancreatic cancer treatment.[118,133–135] Various compounds have gained popularity as HDAC inhibitors, which operate by blocking substrate access to the enzymes and thereby induce cell-cycle arrest and apoptosis in vitro and also have been reported to be successful for in vivo investigations.[136–139] HDAC inhibitors can be structurally grouped into at least four classes: hydrox-amates, cyclic peptides, aliphatic acids and ben-zamides.[140] The most common HDAC inhibitors known to block HDAC activity are tri-chostatin A (TSA)[141] and suberoylanilide hydroxamic acid (SAHA).[124,142–144] A number of other inhibitors like SNDX-275, MGCD0103 and valproic acid[145,146] have also been reported to show selective inhibition effects on HDAC class I and IV.[147] Healthy cells do not normally get affected when treated with HDAC inhibitors, whereas cancer cells have been reported to exhibit inhibited differentiation and undergo cell death.[143,148] The mechanism of action of HDAC inhibitors are inferred to be due to altered gene expression and changes in non-histone proteins via regulation at the epigenetic and post-translational modification levels. HDAC inhibitors also induce upregulation of the cell cycle gene p21, blocking the CDK complexes and leading to apoptosis via cell cycle arrest.[149,150]

Apoptosis induced by HDAC inhibitors is often seen to be simultaneous with the activation of caspases although SAHA has been proven to induce cell death in its absence; whereas, other HDAC inhibitors require activated caspases to degrade chromosomal DNA.[151]

In this work we aim to show a substrate for HDAC-8 which is an acetylated block copolymer comprising a polyethylene glycol and a polylysine block. Upon acetylation of the lysine residues these polymers are able to form self-assembled structures owing to the distinct hydrophobic-hydrophilic blocks when dissolved in a non-selective solvent and then nano precipitated to a selective (hydrophilic solvent).

Our hypothesis is to provide a large number of acetyl groups to the HDAC enzymes in the cancer microenvironment. This should interfere with the deacetylation of the histone proteins of the cancer cells and alter epigenetic pathways. Lysine was selected as it can be easily acetylated via chemical alteration and HDAC enzymes are largely specific for acetylated lysine residues. These lysine residues are normally found throughout histone proteins that surround DNA and ultimately help regulate DNA transcriptional activity. While HDAC is acting on the nanoparticles acetylated lysines, an encapsulated drug within this nano-structure will rapidly release as HDAC enzymes deacetylate the lysine residues leading to collapse of the nanoparticle. To the best of our knowledge such a system has not been devised earlier although various PEGylated nanocarriers for the delivery of HDAC inhibitors have been reported.[78,152,153]

Results and Discussion

Self-assembly of polymersomes. To investigate if the acetylated polymers would form self-assembled structures at the molecular scale, we used fluorescence based measurements with pyrene as a probe to determine the critical aggregation concentration (CAC) of the copolymers. The ratio of the first (λ_{373} nm) and third (λ_{384} nm) peaks in the fluorescence emission spectra of

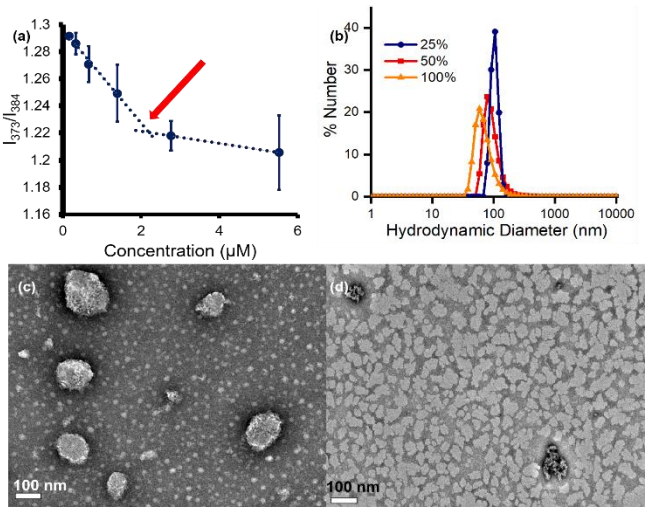

Figure 16. Characterization. (a) CAC plot of the acetylated PEG-b-polylysine (b) Particle size distribution of the different functionalization degrees of the polymers, (c) TEM image of the 100 % functionalized polymersome pre incubation and (d) Post overnight incubation with HDAC8.

pyrene indicate the stability of assembled structures. We observed that the ratio of I_{373}/I_{384} decreased with increasing concentration after which it remained almost the same (Figure 16a). The CAC value of the larger length polymer (n=200) was determined to be 2.2×10^{-6} M and CAC for the smaller polymer as 5.26×10^{-6} M. This indicate the minimum concentration for these polymers to form stable self-assembled structures is in the micro molar range. The copolymers were found to form self-assembled polymersomes under nanoprecipitation condition from DMSO to an aqueous buffered solution of pH 7.4. They exhibited an average diameter of 108 ± 10.7 nm (n = 5) when formed under similar conditions (Figure 16b). These polymersome solutions were found to be stable for up to 4 weeks when stored at 4 °C. When incubated with HDAC8 at 37°C overnight these polymersomes showed a reduction in size. This observation is possibly due to the breakdown of the acetyl groups by HDAC8 and the collapse of the self-assembled structures due to the loss of the hydrophobic block. Transmission electron microscopy (TEM) showed a distinct population of polymersomes at pH 7.4. The particles post incubation

with HDAC8 did not show any discernible structures on the TEM grid as they had collapsed due to the deacetylation leading to the loss of hydrophobicity of the polylysine block. (Figure 16c, d).

Polymersomes as substrate for HDAC8. We then checked whether the acetylated polymersomes would be a substrate for HDAC8 enzymes. A fluorimetric assay was performed using the Fluor De Lys kit where the HDAC8 enzyme was treated with Flour De Lys and different concentrations of polymersomes. This kit utilizes an acetylated lysine residue and after being deacetylated will produce fluorescence upon adding a developer reagent. The emission spectra is then monitored over a period of time. It was observed that with increasing polymersome concentration the emission intensity decreased which indicates lower binding to the Fluor De Lys substrate and increasing binding to the acetyl groups of the polymersomes (Figure 17a).

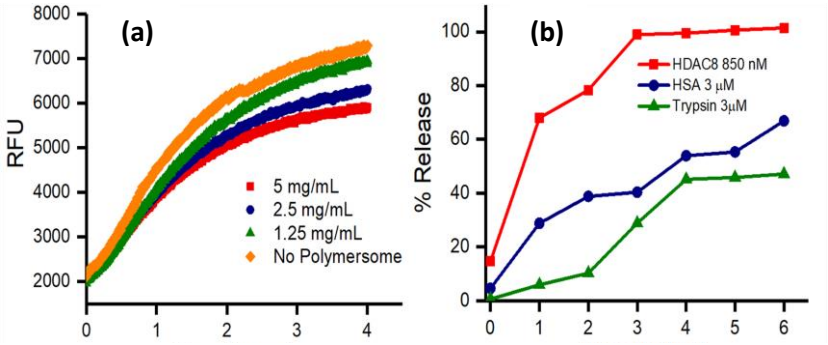

Figure 17. Fluor De Lys. (a) Emission intensity plot of the Flour De Lys assay in presence of different polymersome concentrations and without it **(b)** Release plot of encapsulated 5(6) carboxyfluorescein in the presence of 850 nM HDAC8, 3 μM HSA and 3 μM Trypsin.

Enzyme mediated release of encapsulated dye. To investigate the encapsulation and release properties of the acetylated polymersomes, a model dye (5(6)carboxyfluorescein) was encapsulated within the polymersomes by co-precipitation as described in the previous section. The release of the dye from the polymersomes was studied at different conditions by monitoring the emission spectra of the released dye by exciting it at a particular wavelength (492 nm) and

plotting the emission intensity at 517 nm as a function of time to calculate the percentage release. The release experiments were carried out in the presence of 850 nM HDAC8 enzyme, 3 µM Human Serum Albumin (HSA) and 3 µM trypsin (concentrations derived from standardizing the Fluor De Lys assay). The release was monitored for a period of 6 hours and it was observed that almost 100% of the dye was released in the presence of HDAC8 at the end of 3 hours while for HSA and trypsin around 35-40% of the dye content was released at the same time frame (Figure 17b). This led us to infer that the rate of release of the encapsulated cargo is faster in presence of HDAC8 than other proteins and enzymes, which is an indication of some specific interactions between the enzyme and the polymersomes in all probability mediated via the cleaving of the acetyl groups by the enzymes. The release of the encapsulated dye in presence of trypsin and HSA can be attributed to a non-specific interaction and a diffusion based release due to osmotic difference.

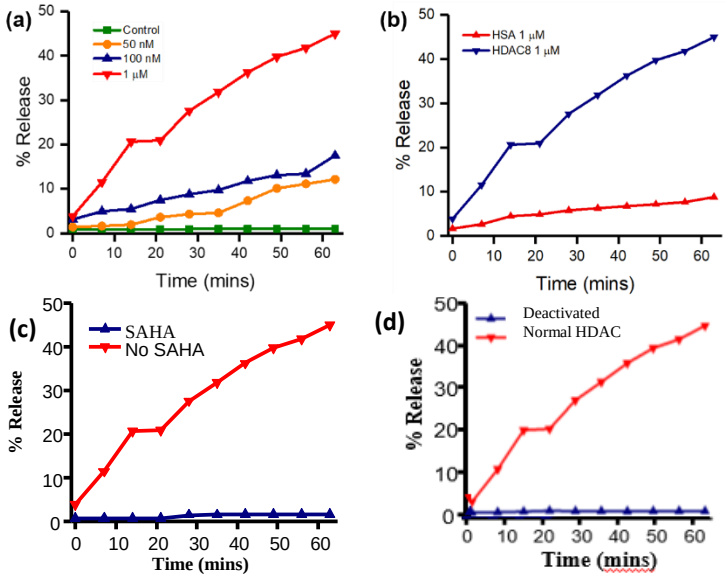

Figure 18. Release with HDAC8. (a) Release plot of encapsulated dye at various HDAC8 concentrations and **(b)** Release plot of 5(6)carboxyfluorescein in the presence of 1 µM HDAC8 and HSA. **(c)** Evolution of carboxyfluorescein release in the presence and absence of SAHA and **(d)** Release profile of the dye in the presence of activated and deactivated enzyme (1 µM).

We narrowed down the time of release to 1 hour with monitoring at smaller time intervals in order to study the kinetics of release better. These experiments were carried out with different HDAC8 concentrations as well as the same concentration for both HSA and HDAC in order to check the specificity of the enzymes in mediating this release. We observed there was a concentration dependent release. HDAC8 at the highest concentration (1 μM) was able to release almost 50% of the dye at the end of one hour. Whereas a lower 100 nM enzyme concentration release was only 15% (Figure 18a). This confirms our hypothesis that the greater the number of enzymes available to the substrate to cleave the acetyl groups the faster the collapse of the self-assembly and the greater release of dye. When treated with HSA there was less than 10% dye release at the end of one hour (Figure 18b), which further confirms the release of the dye is in fact enzyme mediated and any release observed with other substances (trypsin or HSA) was due to the diffusion of the dye across the membrane and is nonspecific in nature. Furthermore, to investigate whether the release profile had an impact in the presence of an inhibitor we added 1 μM SAHA along with the enzyme and monitored the release of the encapsulated cargo (Figure 18c). We observed that there was almost total suppression of release of carboxyfluorescein in presence of the inhibitor. This leads to us infer that the release observed earlier was enzyme specific and in the presence of the inhibitor there are few enzymes available to cleave off the acetyl groups thereby exhibiting almost no increase in emission intensity over time. A similar observation occurred when the polymersomes were treated with deactivated HDAC8 enzymes (Figure 18d). Both these results indicate that the enzyme in its active form interacts with the polymersomes and destabilize the self-assembled structures leading to a total collapse of the nanostructures and release of the encapsulated cargo.

Enzyme mediated release of anti-cancer drug. We wanted to check the potency of our system to encapsulate and release a hydrophobic anti-cancer drug (napabucasin) known for its potency to induce cell death in cancer stem cells by a STAT3 inhibition mechanism.[73,154] The polymersomes were found to have an encapsulation efficiency of 58.5% and a loading content of 13.5%. The polymersomes aexhibited an enzyme catalyzed temporal release (Figure 19) with almost 100% of the drug released at the end of 3 hours. This observation is in line with the dye release observed with 1 μM enzyme and further corroborates the hypothesis that the disruption of the self-assembly in the presence of HDAC enzymes will lead to the release.

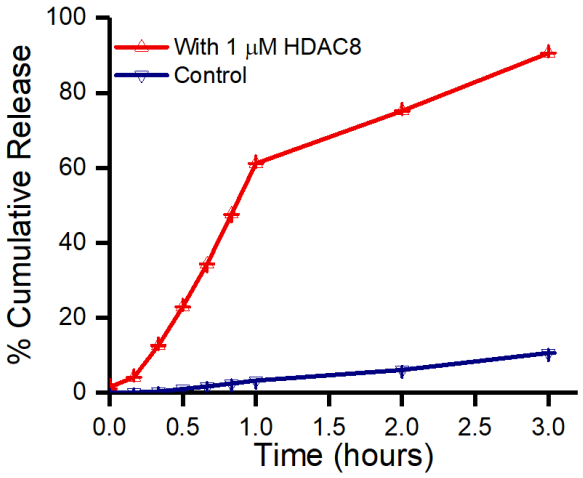

Figure 19. Release of Napabucasin in the presence of HDAC8

Cellular studies and cytotoxicity measurements. We first checked for toxicity of the polymer alone at concentrations 10-20 times higher than those used for drug encapsulated experiments (Figure 20a). The lack of cellular toxicity at these levels would indicate that we are in fact activating the enzyme as a substrate and not completely inhibiting its activity, which has been shown to not only initiate cell death but also produce significant side effects in human trials.[155,156] These findings are also consistent with previous studies that have shown little effect in solid tumor cell lines with HDAC specific inhibitors.[157] The unencapsulated napabucasin was

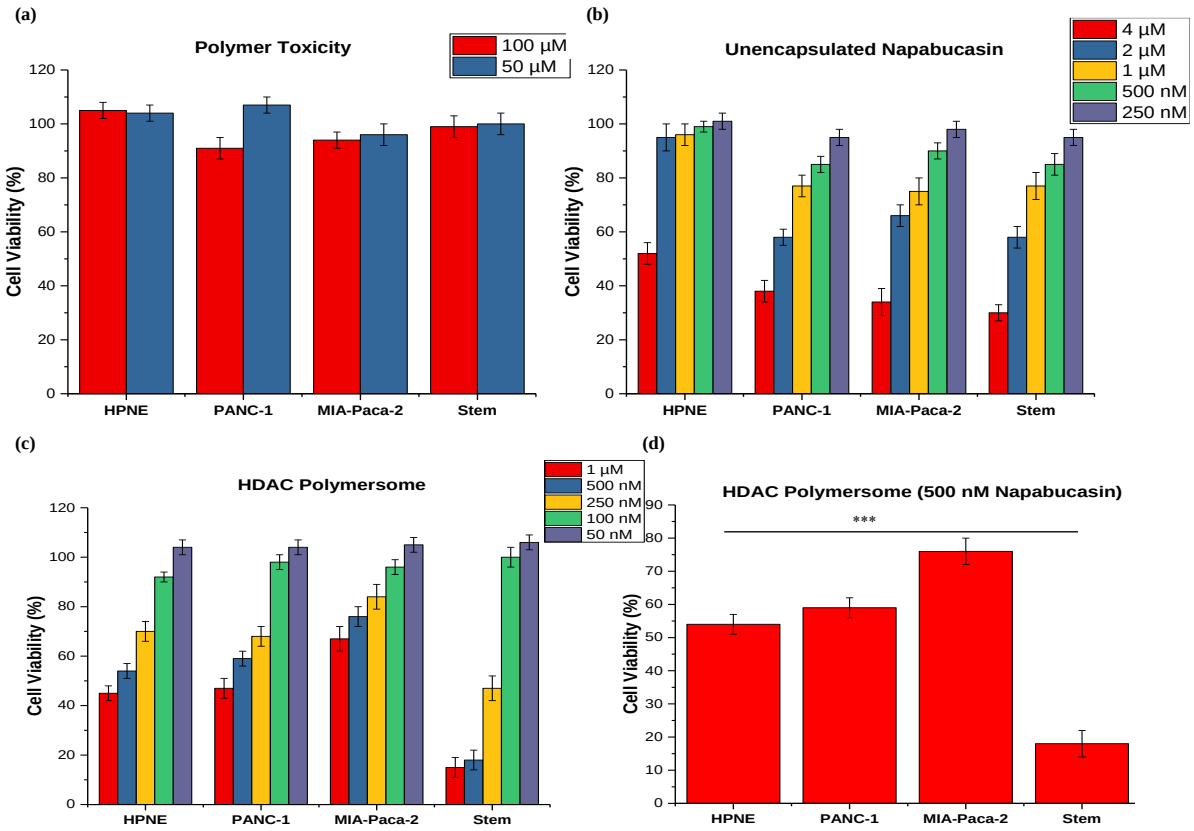

Figure 20. Cellular Toxicity Studies. (a) HDAC NP (b) unencapsulated napabucasin at varying concentrations. (c) HDAC NP with napabucasin encapsulated and (d) comparison between cell lines treated with HDAC NP at 500 nM napabucasin concentration.
*** p-value <0.001 n=6

tested at varying concentrations (Figure 20b). A dose dependent response was seen in the cancerous cell lines while the normal HPNE cells lacked a significant response until concentrations were greater than 2 µM. This lack of response from HPNE is consistent with a previous study that targeted STAT3 as these cells appear to be less dependent on this protein for proliferation.[158] Most intriguing, is what happens when napabucasin is encapsulated into the HDAC polymersomes system. We see a near 10-fold increase in potency and a powerful cytotoxic effect, especially in the stem cells (Figure 20 c/d). A potential mechanism for this increased efficacy may relate to an HDAC8 and STAT3 co-repressor complex identified by Kang et al in colon cancer cells.[159] Where HDAC8 and STAT3 complex and repress BMF's (Bcl-2 modifying factor) apoptotic effect. The HDAC8 protein levels (Figure 21.) seen in each

cell line have a correlation coefficient of 0.9 when comparing the amount of protein to cellular viability. This indicates the amount of HDAC8 protein that is normally made within each cell plays a vital role in cell survival and when this protein is low, cells are more susceptible.

The dose response curves were made by averaging at least three repeats at various drug concentrations. The free napabucasin needed significantly higher doses to produce the same effect as seen in the HDAC8 nanoparticle formulations (Appendix, Figure 8). A dose of 1-2 µm was needed to see significant cell toxicity and death in the free drug group and a more linear dose-response is seen as more drug is then able to diffuse into the cell and begin acting on the STAT3 proteins. When napabucasin is encapsulated into the HDAC8 nanoparticle it allows for a more rapid and higher initial accumulation of the drug inside of the cell. This produces a more sigmoidal curve as STAT3 within the cell is quickly inhibited leading to downstream apoptosis. Also of note, is the slope of the curves for HDA8 nanoparticle treated cells correlates to the relative expression of STAT3 in these cells. A steeper curve, indicating higher toxicity, is seen in the cell lines with less STAT3 protein.

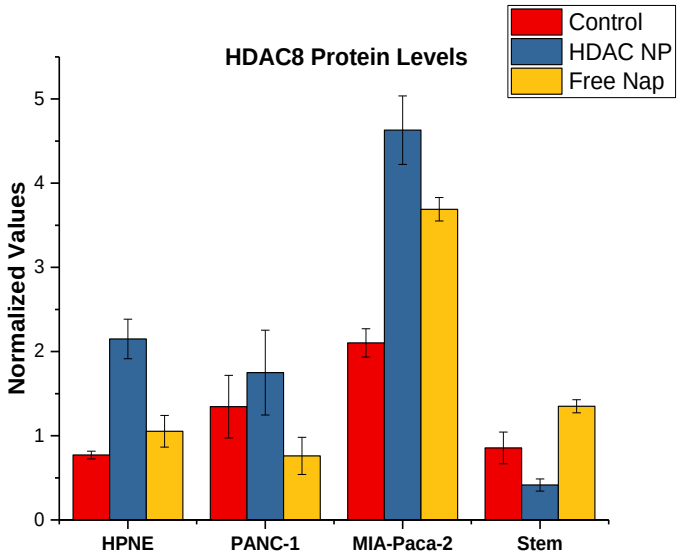

Figure 21. HDAC8 Protein Levels. Relative amount of HDAC8 protein using a cell based ELISA. n=8

Conclusion

HDAC inhibitors have, so far, shown limited efficacy in treatment of solid tumors.[157] An exact biological reason for this lack of efficacy is yet to be determined. However, we have presented a novel polymersome substrate for HDAC enzymes as an alternative to full inhibition. Composed of block co-polymers with lysine residues, the polymersomes are acetylated to form self-assembled structures with an average diameter of 100 nm. These polymersomes were found to be an active substrate for HDAC8 enzymes and likely other class I HDACs that were not tested. The polymersomes were capable of both encapsulating and releasing encapsulated cargo (drugs and dyes) in an enzyme mediated release in a temporally controlled fashion. Additionally, napabucasin, when encapsulated into the polymersomes showed a 10-12 fold increase in potency. The increased cytotoxicity could be accounted for by HDAC8 and STAT3's corepressor complex that prevents transcription of BMF. Inhibition of both HDAC8 and STAT3 would then allow for increased BMF leading to enhanced apoptosis. HDACs are ubiquitous among cells, but their exact role seems to be slightly different, especially among cancer types and even cell types within these cancers. Targeting HDAC enzymes appears to be a promising strategy for cancer treatment whether it is inhibition or as a mechanism for drug release. Further development and a greater understanding of the epigenetic biology is warranted.

Materials and Methods

Materials. PEG-b-polylysine was purchased from Alamanda polymers, all other chemicals were purchased from Sigma-Aldrich, and anhydrous solvents were purchased from VWR, EMD Millipore. Fluor De Lys® HDAC fluorometric activity assay kit was obtained from Enzo Life Sciences. ^{1}H NMR Spectra were recorded using a Bruker 400 MHz spectrometer using TMS as the internal standard. IR Spectra were recorded using an ATR diamond tip on a Thermo Scientific Nicolet 8700 FTIR instrument. DLS measurements were carried out using a

Malvern instrument (Malvern ZS 90). UV− visible and fluorescence spectra were recorded using a Varian UV−vis spectrophotometer and a Fluoro-Log3 fluorescence spectrophotometer, respectively. TEM studies were carried out using a JEOL JEM2100 LaB6 transmission electron microscope (JEOL USA) with an accelerating voltage of 200 keV.

Acetylation of PEG-b-Polylysine. Acetylation of PEG-b-polylysine was carried following the procedure mentioned by Thoma et al.[160], with slight modification, 100 mg (0.0026 mmol) of the PEG-b-polylysine was dissolved in a 4:1 DMF: 2,6-Lutidine solution and cooled in an ice bath. To this a 1 mL DMF solution containing 0.526 mmol acetic anhydride was added slowly. The reaction mixture was stirred at 0°C for 18 hours and precipitated into cold diethyl ether followed by centrifugation at 8000 rpm for 30 minutes with centrifugation step repeated twice to provide a higher yield. The polymers were then characterized using ^{1}H NMR spectroscopy. Different levels of acetylation were used for the polymer with 200 lysine units and the one with maximum functionalization was chosen due to its optimal size. In order to compare the effect of the number of lysine residues and varying chain lengths a similar study was conducted with 100 lysine residues and 100% functionalization.

Determination of the degree of functionalization. To determine the number of lysine residues that have been acetylated, a ninhydrin test was performed on the starting material and the products.[154] Briefly, 2.5 mg of the polymers were dissolved in 2.5 mL of DMSO to which a few drops of freshly prepared ninhydrin solution (200 mg of ninhydrin in 10 mL ethanol) was added and heated in a water bath at 85°C till color development was observed. The absorbance of each sample was measured and the percentage functionalization was calculated using the following equation:

$$mg\ of\ \alpha - amino\ acid = \frac{Abs_{test} - Abs_{blank}}{\mathrm{E}Abs_{stanard} - Abs_{blank}}$$

Preparation of HDAC8 enzymes and assay buffer. The cDNA containing plasmid (mammalian expression vector pCMV-SPORT) was purchased from Open Biosystems Huntsville (clone ID 5761745). The HDAC-8 gene was amplified by PCR reaction using forward and reverse primers. Following ligation of the PCR product with pLIC-His expression vector (obtained as a gift from Prof. Stephen P. Bottomley, Monash University, Australia), the recombinant plasmid (pLIC-His6-HDAC8) was transformed into *E. coli* BL21 codon plus DE3 (RIL) chemically competent cells (purchased from Stratagene) for expression of the HDAC-8 enzyme. The transformed cells cultured in LB medium at 37C to reach OD600. At this point the culture supplemented by 100 µM ZnCl2 and the culturing continued at 16C for 16 additional hours. Cells harvested by centrifugation at 5000 rpm. The pellet was sonicated using lysis buffer. The resulting lysate centrifuged (15000 g for 30 min at 4C) and filtered to remove cell derbies. Pure HDAC-8 enzyme obtained using HisTrap column on AKTA purifier UPC 10 (GE healthcare Life Sciences). SDS-PAGE agarose gel and catalytic activity analysis confirmed the presence of the HDAC-8 enzyme. The HDAC8 assay buffer had the following composition: 50 mM Tris-HCl buffer, containing 137 mM NaCl, 2.7 mM KCl, 1 mM MgCl2, 1 mg/ml BSA, pH 7.5 while the HDAC8 lysis buffer comprised 50 mM Tris-HCl, 150 mM KCl, 3 mM MgCl2, 1mM 2-mercaptoethanol, 1 mM PMSF (Phenylmethylsulfonyl fluoride) and 0.25 % Triton X-100, pH 8

Encapsulation of 5(6) carboxyfluorescein. 5(6)Carboxyfluorescein was encapsulated by the following procedure, briefly, 10 mg of the polymer and 1 mg of 5,6-carboxyfluorescein were dissolved in 250 µL DMSO and was then added dropwise to a 750 µL PBS buffer solution under magnetic stirring. This was left stirring for an hour at room temperature followed by dialysis (MWCO 1-1. 5 kDa) against 800 mL PBS buffer with regular media change till no

further discoloration of the media was observed. 20 μL of Triton was added to disintegrate the polymersome and the fluorescence emission intensity was measured for total release after disintegration. The cumulative percentage release was plotted versus elapsed time. Percentage release was calculated using the following equation:

$$\% \, release = \frac{\text{Emi intensity after rel} - \text{Emi intensity before rel}}{\text{Emi intensity after Triton rel} - \text{Emi intensity before rel}} \times 100$$

Determination of the critical aggregation concentration (CAC) of the polymers. To evaluate the aggregate forming capacity of the copolymers and to estimate their systemic stability, we determined the critical aggregation concentration (CAC) of the synthesized architectures. A stock solution of 0.1 mM pyrene in dichloromethane was prepared. An aliquot of 10 μL of this solution was taken in a set of vials, and dichloromethane was allowed to evaporate by air-drying. To each of these vials, various measured amounts of the acetylated polymers were added (from a stock solution of 10 μM) so that the concentrations varied from 0.15 to 5.5 μM and the final concentration of pyrene in each vial remained 1 μM. The vials were sonicated for 1 h 30 min and then allowed to stand for 3 h before recording the fluorescence spectra. The fluorescence emission spectra were acquired at an excitation wavelength of 337 nm with slits of 2.5 nm (for both excitation and emission). The ratio of the intensities at 373 and 384 nm were plotted against the concentration of the polymer, and the inflection point of the curve was used to determine the CAC.[71,150]

Preparation of polymersomes. We employed nanoprecipitation, also known as the solvent shifting method, from a selective solvent (DMSO) to a nonselective solvent (buffer). The acetylated polymers were dissolved in 250 μL of DMSO, and the solution was added dropwise to 750 μL of PBS buffer (pH 7.4). The resultant solution was transferred to a float-a-lyzer dialysis

device (MWCO 3.5−5 kDa) and dialyzed against 800 mL PBS buffer (pH 7.4) overnight with constant shaking at moderate speed. For the napabucasin encapsulated polymersome system, 10 mg of the polymer and 5 mg of napabucacin were dissolved in 250 μL of DMSO and added slowly dropwise to a separate vial containing 750 μL of PBS (pH 7.4) with constant stirring. The solution was allowed to stir overnight followed by filtration using an ultracentrifuge filter (MWCO 3.5−5 kDa) at 5000 rpm for 3 hours to prepare the purified polymersomes. Then the resulting polymersome suspension was dispersed in chilled (4 °C) buffer to a concentration of 10 mg/mL. Polymersomes were tested for size prior to use to confirm formation and observe for aggregation. The filtrate was used to quantify the amount of drug encapsulated. The encapsulation efficiency was calculated using the following equation:

$$Encapsulation\ efficiency\ (\%) = \frac{\text{Amount of drug added} - \text{Amount of drug in filtrate}}{\text{Amount of drug added}} \times 100$$

Particle size and zeta potential analysis of polymersomes. The hydrodynamic diameters of resulting polymersomes prepared from the acetylated block copolymers were determined using Dynamic Light Scattering (DLS) at a scattering angle of 90°. For zeta potential measurements a sample concentration of 10 mg/mL was used and the zeta potential was determined in terms of electrophoretic mobility by taking an average of 5 readings. For all of these measurements, the sample solution was filtered using a 0.45 μm PES filters.

Size analysis using TEM imaging. A drop of polymersome sample (obtained from the acetylated polymers) was placed on a 300-mesh Formvar carbon coated copper TEM grid (Electron Microscopy Sciences) for 1 min and wicked off. Phosphotungstic acid 0.1%, pH adjusted to 7− 8, was dropped onto the grid and allowed to stand for 2 min and then wicked off.

Polymersomes incubated with HDAC8 at have been investigated for their microstructure by TEM at 200 keV.

Fluor De Lys® HDAC fluorometric assay. The assay was performed on a microplate reader. Varying polymersome concentrations were used and the HDAC8 concentration was optimized to be 850 nM. The Fluor De Lys® substrate concentration was maintained at 200 µM. The excitation wavelength was 360 nm and the emission recorded at 460 nm. The emission spectra was monitored for a period of 4 hours.

In vitro release of napabucacin. In vitro drug release was studied at two different conditions in the presence of 1µM HDAC8 and in its absence using the same buffer solution. An aliquot of 1 mL of the drug encapsulated polymersomes was taken in different Float-a-lyzer (MWCO 3.5−5 kDa) chambers against 5 mL of media. After a specified time interval, 1 mL of sample was withdrawn and replaced with the same volume of fresh media. The samples were then analyzed for napabucacin concentration using UV−vis spectroscopy.

Cellular studies. In-vitro studies were carried out using four cell variants. HPNE, PANC-1, and MIA-Paca-2 cell lines were obtained from American Type Tissue Culture (ATCC) and subsequently maintained and passaged according to ATCC recommendations. The fourth cell variant, are patient-derived xenograft pancreatic cancer stem cells obtained from Celprogen. The stem cells were maintained and passaged using Celprogen recommended media, flasks, and plates. For all studies, a passage number of less than 10 was used, except for the stem cells where only passages below 5 were used.

In-vitro cytotoxicity. Cells were seeded in a 96-well plate at a density of 10,000 cells/well and were allowed 24 hours of incubation prior to adding treatments. Polymersomes containing napabucasin were suspended in serum free cell culture media and added to their

respective wells. 24 hours post treatment, the cells were washed 3x with phosphate buffered saline and a 10% concentration of Alamar Blue (Bio Rad) was used to determine cell viability/cytotoxicity.

Estimation of HDAC8 protein levels. An HDAC8 cell-based ELISA kit, obtained from Abnova, was used to quantify the relative levels of HDAC8 protein in each cell variant. Values were normalized using GAPDH and crystal violet cell stain.

Acknowledgements

We would like to thank Dr. Mohiuddin Quadir and Dr. Priyanka Ray for their help in making this work possible.

CONCLUSION

The human understanding of medicine has come a long way from ingesting ground up animal dung and plant matter. Our knowledge of biology, biochemistry, and science in general would not be where it is without the sacrifices, failures, and breakthroughs that came before us. The United States national nanotechnology initiative that began in the year 2000, jump started the field of nano research. Nanomaterials now encompass many scientific disciplines from chemistry and biology to physics and engineering. We are nearing a time of exponential growth in nanomedicine and nanomaterials as we have learned basic design principles, and have seen their vast potential. This potential is seen in our hypoxia responsive nanoparticles that were able to decrease tumor growth by as much as 260% or the potential of increasing efficacy as our HDAC responsive nanoparticles showed a 10-fold greater potency.

Chemical modifications to nanoparticles have further effected the way nanoparticles interact with our bodies, leading to significant increases in circulation time and ability to target cells expressing specific receptors. Environment responsive qualities further add specificity and can allow for increased accumulation either at the therapeutic site of action or the tumor site in general. Inclusion of these alterations along with consideration of basic design principles (drug selection, biocompatibility, and size) produced significant tumor core necrosis, tumor suppression, and no apparent severe toxicity in an animal model of disease. However, this represents the response from only one genetic line. In clinical medicine we encounter wide variability of genetics that will play a role in treatment outcome. The HDAC responsive polymersomes tested four different cell lines, each with their own genetic profiles and mutations. Treating different cells led to significantly altered reactions to treatment depending on cell

characteristics (Figure 20). We even saw that the same cells (BxPC-3) will respond differently to treatment depending on their oxygenation (Figure 6).

A nano-sized approach to disease forces us think small to get big results. We have a plethora of small therapeutic molecules that have shown promise through cellular testing, small animal models, and even into clinical trials. Yet, failure results in greater than 90% of cancer clinical trials. Our studies show that we can increase effectiveness of these agents that had previously showed promise, but failed due to severe side effects or failure to demonstrate improved outcomes. Gemcitabine, for example, has been used for over 20 years (FDA approved 1996) and our simple encapsulation protocol led to a more effective formulation that reduced tumor size 42% more than standard gemcitabine. Doxorubicin, known for cardiotoxicity, was re-formulated as a nanoparticle formulation to offset cardiotoxic effects. Many other FDA approved medications currently exist that have black box warnings for various toxicities that may also be able to be re-formulated as a more targeted nanoparticle therapy with lower incidence of toxicity.

For the future of nanomedicine, there are many non-biological aspects that also need to be considered. During drug development, there will be added difficulties in formulation; can we control aggregation, maintain consistent nanoparticle size, stability and storage requirements. Safety, especially in patients with decreased liver and kidney function. Cost, a factor that is continually highlighted with new treatments. Higher development costs along with potentially shorter expiration dates caused by lower stability of the nanoparticle vs. dried powder of the drug will lead to higher costs to patients.

The mass production of nanoparticles will be necessary to facilitate wide use of nanomedicine therapies. However, this is easier said than done. Changes in speed or agitation of mixtures significantly effects the nanoparticle size and drug loading can become hindered at

higher volumes of production.[161,162] New processes such as flash nanoprecipitation are able to produce tunable particles sizes in the range of 50-500 nm with variability under 10%. Yet this technique is not feasible for all nanoparticle forms (currently optimized for polymeric nanoparticles). As with many manufacturing processes nanomedicine production may not have a universal standard of production and new technologies and strategies are being developed to address this looming problem.

Today, many diseases and conditions have available medications that work very well, have low side effects, and low costs. A nano formulation of every drug for every disease is not a realistic or even practical idea. However, many diseases exist that require a more non-traditional approach. The blood-brain-barrier, makes hydrophilic drugs useless for treatment without a way of penetration, which can be done using nanoparticles. Gene therapies require delivery of sensitive DNA modulating agents, which can be done using nanoparticles. The list of possible uses for nanomedicine continues to grow every year. Continued experimentation, ingenuity, and desire to help people will push nano formulations to clinical use and beyond.

REFERENCES

1. Jatzkewitz H. Incorporation of Physiologically-Active Substances into a Colloidal Blood Plasma Substitute. Incorporation of Mescaline Peptide into Polyvinylpyrrolidone. *Hoppe-Seyler's Z Physiol Chem*. 1954;297(3-6):149-156.

2. Bangham AD, Horne RW. Negative Staining Of Phospholipids And Their Structural Modification By Surface-Active Agents As Observed In The Electron Microscope. *J Mol Biol*. 1964;8:660-668. doi:10.1016/s0022-2836(64)80115-7

3. Scheffel U, Rhodes BA, Natarajan TK, Wagner HN. Albumin Microspheres For Study Of The Reticuloendothelial System. *J Nucl Med*. 1972;13(7):498-503.

4. Matsumura Y, Maeda H. A New Concept For Macromolecular Therapeutics In Cancer Chemotherapy: Mechanism Of Tumoritropic Accumulation Of Proteins And The Antitumor Agent Smancs. *Cancer Res*. 1986;46(12 Pt 1):6387-6392.

5. Ventola CL. Progress in Nanomedicine: Approved and Investigational Nanodrugs. *P T*. 2017;42(12):742-755.

6. Alizadeh AA, Aranda V, Bardelli A, et al. Toward Understanding And Exploiting Tumor Heterogeneity. *Nat Med*. 2015;21(8):846-853. doi:10.1038/nm.3915

7. Marusyk A, Almendro V, Polyak K. Intra-tumour heterogeneity: a looking glass for cancer? *Nat Rev Cancer*. 2012;12(5):323-334. doi:10.1038/nrc3261

8. Meacham CE, Morrison SJ. Tumour Heterogeneity And Cancer Cell Plasticity. *Nature*. 2013;501(7467):328-337. doi:10.1038/nature12624

9. Apte M, Haber P, Darby S, et al. Pancreatic Stellate Cells Are Activated By Proinflammatory Cytokines: Implications For Pancreatic Fibrogenesis. *Gut*. 1999;44(4):534-541.

10. Cai M-H, Xu X-G, Yan S-L, et al. Depletion of HDAC1, 7 and 8 by Histone Deacetylase Inhibition Confers Elimination of Pancreatic Cancer Stem Cells in Combination with Gemcitabine. *Sci Rep*. 2018;8(1):1-11. doi:10.1038/s41598-018-20004-0

11. Rafiyath SM, Rasul M, Lee B, Wei G, Lamba G, Liu D. Comparison of Safety and Toxicity of Liposomal Doxorubicin vs. Conventional Anthracyclines: a Meta-Analysis. *Experimental Hematology & Oncology*. 2012;1(1):10. doi:10.1186/2162-3619-1-10

12. Immordino ML, Dosio F, Cattel L. Stealth Liposomes: Review Of The Basic Science, Rationale, And Clinical Applications, Existing And Potential. *Int J Nanomedicine*. 2006;1(3):297-315.

13. Suk JS, Xu Q, Kim N, Hanes J, Ensign LM. PEGylation As A Strategy For Improving Nanoparticle-Based Drug And Gene Delivery. *Adv Drug Deliv Rev*. 2016;99(Pt A):28-51. doi:10.1016/j.addr.2015.09.012

14. Walkey CD, Olsen JB, Guo H, Emili A, Chan WCW. Nanoparticle Size And Surface Chemistry Determine Serum Protein Adsorption And Macrophage Uptake. *J Am Chem Soc*. 2012;134(4):2139-2147. doi:10.1021/ja2084338

15. Ehrenberg M, McGrath JL. Binding Between Particles And Proteins In Extracts: Implications For Microrheology And Toxicity. *Acta Biomaterialia*. 2005;1(3):305-315. doi:10.1016/j.actbio.2005.02.002

16. Aggarwal P, Hall JB, McLeland CB, Dobrovolskaia MA, McNeil SE. Nanoparticle Interaction With Plasma Proteins As It Relates To Particle Biodistribution, Biocompatibility And Therapeutic Efficacy. *Advanced Drug Delivery Reviews*. 2009;61(6):428-437. doi:10.1016/j.addr.2009.03.009

17. Hadjidemetriou M, Al-Ahmady Z, Mazza M, Collins RF, Dawson K, Kostarelos K. In Vivo Biomolecule Corona around Blood-Circulating, Clinically Used and Antibody-Targeted Lipid Bilayer Nanoscale Vesicles. *ACS Nano*. 2015;9(8):8142-8156. doi:10.1021/acsnano.5b03300

18. Dash BC, Réthoré G, Monaghan M, Fitzgerald K, Gallagher W, Pandit A. The Influence Of Size And Charge Of Chitosan/Polyglutamic Acid Hollow Spheres On Cellular Internalization, Viability And Blood Compatibility. *Biomaterials*. 2010;31(32):8188-8197. doi:10.1016/j.biomaterials.2010.07.067

19. Pham CTN, Thomas DG, Beiser J, et al. Application of a Hemolysis Assay For Analysis Of Complement Activation By Perfluorocarbon Nanoparticles. *Nanomedicine*. 2014;10(3):651-660. doi:10.1016/j.nano.2013.10.012

20. Robbins GR, Roberts RA, Guo H, et al. Analysis of Human Innate Immune Responses To Print Fabricated Nanoparticles With Cross Validation Using A Humanized Mouse Model. *Nanomedicine*. 2015;11(3):589-599. doi:10.1016/j.nano.2014.11.010

21. Du B, Yu M, Zheng J,Transport and Interactions Of Nanoparticles In The Kidneys. *Nature Reviews Materials; London*. 2018;3(10):358-374. doi:http://dx.doi.org.ezproxy.lib.ndsu.nodak.edu/10.1038/s41578-018-0038-3

22. Tsoi KM, MacParland SA, Ma X-Z, et al. Mechanism of Hard Nanomaterial Clearance By The Liver. *Nat Mater*. 2016;15(11):1212-1221. doi:10.1038/nmat4718

23. Al CL et. Strategies for The Intracellular Delivery Of Nanoparticles. - PubMed - NCBI. https://www.ncbi.nlm.nih.gov/pubmed/20886124. Accessed September 23, 2019.

24. Li Y, Stroberg W, Lee T-R, et al. Multiscale Modeling And Uncertainty Quantification In Nanoparticle-Mediated Drug/Gene Delivery. *Comput Mech*. 2014;53(3):511-537. doi:10.1007/s00466-013-0953-5

25. Li Y, Lian Y, Zhang LT, et al. Cell and Nanoparticle Transport In Tumour Microvasculature: The Role Of Size, Shape And Surface Functionality Of Nanoparticles. *Interface Focus*. 2016;6(1):20150086. doi:10.1098/rsfs.2015.0086

26. Albanese A, Tang PS, Chan WCW. The Effect Of Nanoparticle Size, Shape, And Surface Chemistry On Biological Systems. *Annu Rev Biomed Eng*. 2012;14:1-16. doi:10.1146/annurev-bioeng-071811-150124

27. Petros RA, DeSimone JM. Strategies in the Design Of Nanoparticles For Therapeutic Applications. *Nat Rev Drug Discov*. 2010;9(8):615-627. doi:10.1038/nrd2591

28. BG et al. USNCTAM Perspectives On Mechanics In Medicine. - PubMed - NCBI. https://www.ncbi.nlm.nih.gov/pubmed/24872502. Accessed September 23, 2019.

29. Decuzzi P, Pasqualini R, Arap W, Ferrari M. Intravascular Delivery Of Particulate Systems: Does Geometry Really Matter? *Pharm Res*. 2009;26(1):235-243. doi:10.1007/s11095-008-9697-x

30. Decuzzi P, Ferrari M. Design Maps For Nanoparticles Targeting The Diseased Microvasculature. *Biomaterials*. 2008;29(3):377-384. doi:10.1016/j.biomaterials.2007.09.025

31. Kulkarni P, Haldar MK, You S, Choi Y, Mallik S. Hypoxia-Responsive Polymersomes for Drug Delivery to Hypoxic Pancreatic Cancer Cells. *Biomacromolecules*. 2016;17(8):2507-2513. doi:10.1021/acs.biomac.6b00350

32. Kulkarni P, Haldar MK, Karandish F, et al. Tissue-Penetrating, Hypoxia-Responsive Echogenic Polymersomes For Drug Delivery To Solid Tumors. *Chemistry*. July 2018. doi:10.1002/chem.201802229

33. Jain RK. Normalization of Tumor Vasculature: An Emerging Concept In Antiangiogenic Therapy. *Science*. 2005;307(5706):58-62. doi:10.1126/science.1104819

34. Sands H, Jones PL, Shah SA, Palme D, Vessella RL, Gallagher BM. Correlation of Vascular Permeability And Blood Flow With Monoclonal Antibody Uptake By Human Clouser And Renal Cell Xenografts. *Cancer Res*. 1988;48(1):188-193.

35. Koong AC, Mehta VK, Le QT, et al. Pancreatic Tumors Show High Levels Of Hypoxia. *International Journal of Radiation Oncology*Biology*Physics*. 2000;48(4):919-922. doi:10.1016/S0360-3016(00)00803-8

36. Rampling R, Cruickshank G, Lewis AD, Fitzsimmons SA, Workman P. Direct Measurement Of Po2 Distribution And Bioreductive Enzymes In Human Malignant Brain Tumors. *International Journal of Radiation Oncology*Biology*Physics*. 1994;29(3):427-431. doi:10.1016/0360-3016(94)90432-4

37. Tumor Oxygenation Predicts for the Likelihood of Distant Metastases in Human Soft Tissue Sarcoma | Cancer Research. http://cancerres.aacrjournals.org/content/56/5/941.short. Accessed February 10, 2019.

38. Pretreatment Oxygenation Predicts Radiation Response In Advanced Squamous Cell Carcinoma Of The Head And Neck - ScienceDirect.

https://www.sciencedirect.com/science/article/pii/S0167814096918113. Accessed February 10, 2019.

39. Okunieff P, Hoeckel M, Dunphy EP, Schlenger K, Knoop C, Vaupel P. Oxygen Tension Distributions Are Sufficient To Explain The Local Response Of Human Breast Tumors Treated With Radiation Alone. *International Journal of Radiation Oncology*Biology*Physics*. 1993;26(4):631-636. doi:10.1016/0360-3016(93)90280-9

40. Höckel M, Knoop C, Schlenger K, et al. Intratumoral pO2 Predicts Survival In Advanced Cancer Of The Uterine Cervix. *Radiotherapy and Oncology*. 1993;26(1):45-50. doi:10.1016/0167-8140(93)90025-4

41. Fyles AW, Milosevic M, Wong R, et al. Oxygenation Predicts Radiation Response And Survival In Patients With Cervix Cancer. *Radiotherapy and Oncology*. 1998;48(2):149-156. doi:10.1016/S0167-8140(98)00044-9

42. Movsas B, Chapman JD, Horwitz EM, et al. Hypoxic regions Exist In Human Prostate Carcinoma. *Urology*. 1999;53(1):11-18. doi:10.1016/S0090-4295(98)00500-7

43. Vaupel P, Höckel M, Mayer A. Detection and Characterization Of Tumor Hypoxia Using Po2 Histography. *Antioxid Redox Signal*. 2007;9(8):1221-1235. doi:10.1089/ars.2007.1628

44. Bertout JA, Patel SA, Simon MC. The Impact Of O2 Availability On Human Cancer. *Nat Rev Cancer*. 2008;8(12):967-975. doi:10.1038/nrc2540

45. Finger EC, Giaccia AJ. Hypoxia, Inflammation, And The Tumor Microenvironment In Metastatic Disease. *Cancer Metastasis Rev*. 2010;29(2):285-293. doi:10.1007/s10555-010-9224-5

46. Semenza GL. Defining the Role of Hypoxia-Inducible Factor 1 in Cancer Biology and Therapeutics. *Oncogene*. 2010;29(5):625-634. doi:10.1038/onc.2009.441

47. Semenza GL. Molecular Mechanisms Mediating Metastasis Of Hypoxic Breast Cancer Cells. *Trends Mol Med*. 2012;18(9):534-543. doi:10.1016/j.molmed.2012.08.001

48. Bailey JM, Alsina J, Rasheed ZA, et al. DCLK1 Marks A Morphologically Distinct Subpopulation Of Cells With Stem Cell Properties In Preinvasive Pancreatic Cancer. *Gastroenterology*. 2014;146(1):245-256. doi:10.1053/j.gastro.2013.09.050

49. Ohara Y, Oda T, Sugano M, et al. Histological and Prognostic Importance of CD44(+) /CD24(+) /EpCAM(+) Expression in Clinical Pancreatic Cancer. *Cancer Sci*. 2013;104(8):1127-1134. doi:10.1111/cas.12198

50. Li L, Borodyansky L, Yang Y. Genomic Instability En Route To And From Cancer Stem Cells. *Cell Cycle*. 2009;8(7):1000-1002. doi:10.4161/cc.8.7.8041

51. Zhang S, Luo X, Wan F, Lei T. The Roles Of Hypoxia-Inducible Factors In Regulating Neural Stem Cells Migration To Glioma Stem Cells And Determinating Their Fates. *Neurochem Res*. 2012;37(12):2659-2666. doi:10.1007/s11064-012-0879-x

52. Semenza GL. Hypoxia-inducible Factors: Coupling Glucose Metabolism And Redox Regulation With Induction Of The Breast Cancer Stem Cell Phenotype. *EMBO J*. 2017;36(3):252-259. doi:10.15252/embj.201695204

53. Sun JC, He F, Yi W, et al. High expression of HIF-2α and its Anti-Radiotherapy Effect In Lung Cancer Stem Cells. *Genet Mol Res*. 2015;14(4):18110-18120. doi:10.4238/2015.December.22.37

54. Corcoran RB, Contino G, Deshpande V, et al. STAT3 Plays a Critical Role in KRAS-Induced Pancreatic Tumorigenesis. *Cancer Res*. 2011;71(14):5020-5029. doi:10.1158/0008-5472.CAN-11-0908

55. Rebouissou S, Amessou M, Couchy G, et al. Frequent in-frame Somatic Deletions Activate Gp130 In Inflammatory Hepatocellular Tumours. *Nature*. 2009;457(7226):200-204. doi:10.1038/nature07475

56. Putoczki TL, Thiem S, Loving A, et al. Interleukin-11 Is the Dominant IL-6 Family Cytokine during Gastrointestinal Tumorigenesis and Can Be Targeted Therapeutically. *Cancer Cell*. 2013;24(2):257-271. doi:10.1016/j.ccr.2013.06.017

57. Direct Reprogramming Of Stem Cell Properties In Colon Cancer Cells By CD44 | The EMBO Journal. http://emboj.embopress.org/content/30/15/3186. Accessed February 10, 2019.

58. Lee TKW, Castilho A, Cheung VCH, Tang KH, Ma S, Ng IOL. CD24+ Liver Tumor-Initiating Cells Drive Self-Renewal and Tumor Initiation through STAT3-Mediated NANOG Regulation. *Cell Stem Cell*. 2011;9(1):50-63. doi:10.1016/j.stem.2011.06.005

59. Loss of Androgen Receptor Expression Promotes a Stem-like Cell Phenotype in Prostate Cancer through STAT3 Signaling | Cancer Research. http://cancerres.aacrjournals.org/content/74/4/1227. Accessed February 10, 2019.

60. Panni RZ, Sanford DE, Belt BA, et al. Tumor-induced STAT3 Activation In Monocytic Myeloid-Derived Suppressor Cells Enhances Stemness And Mesenchymal Properties In Human Pancreatic Cancer. *Cancer Immunol Immunother*. 2014;63(5):513-528. doi:10.1007/s00262-014-1527-x

61. Fukahi K, Fukasawa M, Neufeld G, Itakura J, Korc M. Aberrant Expression of Neuropilin-1 and -2 in Human Pancreatic Cancer Cells. *Clin Cancer Res*. 2004;10(2):581-590. doi:10.1158/1078-0432.CCR-0930-03

62. Karandish F, Froberg J, Borowicz P, Wilkinson JC, Choi Y, Mallik S. Peptide-targeted, Stimuli-Responsive Polymersomes For Delivering A Cancer Stemness Inhibitor To

Cancer Stem Cell Microtumors. *Colloids Surf B Biointerfaces*. 2018;163:225-235. doi:10.1016/j.colsurfb.2017.12.036

63. Yin H, Yang J, Zhang Q, et al. iRGD as a Tumor-Penetrating Peptide For Cancer Therapy (Review). *Molecular Medicine Reports*. 2017;15(5):2925–2930. doi:10.3892/mmr.2017.6419

64. Sugahara KN, Teesalu T, Karmali PP, et al. Tissue-penetrating Delivery Of Compounds And Nanoparticles Into Tumors. *Cancer Cell*. 2009;16(6):510-520. doi:10.1016/j.ccr.2009.10.013

65. Falcone S, Cocucci E, Podini P, Kirchhausen T, Clementi E, Meldolesi J. Macropinocytosis: Regulated Coordination Of Endocytic And Exocytic Membrane Traffic Events. *J Cell Sci*. 2006;119(22):4758-4769. doi:10.1242/jcs.03238

66. Simón-Gracia L, Hunt H, Scodeller P, et al. iRGD Peptide Conjugation Potentiates Intraperitoneal Tumor Delivery Of Paclitaxel With Polymersomes. *Biomaterials*. 2016;104:247-257. doi:10.1016/j.biomaterials.2016.07.023

67. Kadonosono T, Yamano A, Goto T, et al. Cell Penetrating Peptides Improve Tumor Delivery Of Cargos Through Neuropilin-1-Dependent Extravasation. *Journal of Controlled Release*. 2015;201:14-21. doi:10.1016/j.jconrel.2015.01.011

68. Rudin D, Li L, Niu N, et al. Gemcitabine Cytotoxicity: Interaction of Efflux and Deamination. *J Drug Metab Toxicol*. 2011;2(107):1-10. doi:10.4172/2157-7609.1000107

69. Mini E, Nobili S, Caciagli B, Landini I, Mazzei T. Cellular Pharmacology Of Gemcitabine. *Ann Oncol*. 2006;17 Suppl 5:v7-12. doi:10.1093/annonc/mdj941

70. Kulkarni P, Haldar MK, You S, Choi Y, Mallik S. Hypoxia-Responsive Polymersomes for Drug Delivery to Hypoxic Pancreatic Cancer Cells. *Biomacromolecules*. 2016;17(8):2507-2513. doi:10.1021/acs.biomac.6b00350

71. Luo J, Yan R, He X, He J. Constitutive Activation Of Stat3 And Cyclin D1 Overexpression Contribute To Proliferation, Migration And Invasion In Gastric Cancer Cells. *Am J Transl Res*. 2017;9(12):5671-5677.

72. Li Y, Rogoff HA, Keates S, et al. Suppression of Cancer Relapse And Metastasis By Inhibiting Cancer Stemness. *PNAS*. 2015;112(6):1839-1844. doi:10.1073/pnas.1424171112

73. Napabucasin: An Update on the First-in-Class Cancer Stemness Inhibitor | SpringerLink. https://link.springer.com/article/10.1007/s40265-017-0759-4. Accessed October 1, 2019.

74. Suppression Of Prostate Cancer Progression By Cancer Cell Stemness Inhibitor Napabucasin - Zhang - 2016 - Cancer Medicine - Wiley Online Library. https://onlinelibrary.wiley.com/doi/full/10.1002/cam4.675. Accessed October 1, 2019.

75. Loscalzo J. Adaptions to Hypoxia and Redox Stress: Essential Concepts Confounded by Misleading Terminology. *Circ Res*. 2016;119(4):511-513. doi:10.1161/CIRCRESAHA.116.309394

76. Jubb AM, Buffa FM, Harris AL. Assessment of Tumour Hypoxia For Prediction Of Response To Therapy And Cancer Prognosis. *J Cell Mol Med*. 2010;14(1-2):18-29. doi:10.1111/j.1582-4934.2009.00944.x

77. Kulkarni P, Haldar MK, Karandish F, et al. Tissue-Penetrating, Hypoxia-Responsive Echogenic Polymersomes For Drug Delivery To Solid Tumors. *Chemistry – A European Journal*. 2018;24(48):12490-12494. doi:10.1002/chem.201802229

78. Anajafi T, Yu J, Sedigh A, et al. Nuclear Localizing Peptide-Conjugated, Redox-Sensitive Polymersomes for Delivering Curcumin and Doxorubicin to Pancreatic Cancer Microtumors. *Mol Pharm*. 2017;14(6):1916-1928. doi:10.1021/acs.molpharmaceut.7b00014

79. Dan K, Bose N, Ghosh S. Vesicular Assembly And Thermo-Responsive Vesicle-To-Micelle Transition From An Amphiphilic Random Copolymer. *Chem Commun*. 2011;47(46):12491-12493. doi:10.1039/C1CC15663B

80. PEG-b-poly (carbonate)-Derived Nanocarrier Platform With Ph-Responsive Properties For Pancreatic Cancer Combination Therapy. - PubMed - NCBI. https://www.ncbi.nlm.nih.gov/pubmed/30447521. Accessed April 16, 2019.

81. Nahire R, Haldar MK, Paul S, et al. Multifunctional Polymersomes For Cytosolic Delivery Of Gemcitabine And Doxorubicin To Cancer Cells. *Biomaterials*. 2014;35(24):6482-6497. doi:10.1016/j.biomaterials.2014.04.026

82. Toy R, Peiris PM, Ghaghada KB, Karathanasis E. Shaping Cancer Nanomedicine: The Effect Of Particle Shape On The In Vivo Journey Of Nanoparticles. *Nanomedicine (Lond)*. 2014;9(1):121-134. doi:10.2217/nnm.13.191

83. Nagayasu null, Uchiyama null, Kiwada null. The size of Liposomes: A Factor Which Affects Their Targeting Efficiency To Tumors And Therapeutic Activity Of Liposomal Antitumor Drugs. *Adv Drug Deliv Rev*. 1999;40(1-2):75-87.

84. Maeda H. The Enhanced Permeability And Retention (EPR) Effect In Tumor Vasculature: The Key Role Of Tumor-Selective Macromolecular Drug Targeting. *Advances in Enzyme Regulation*. 2001;41(1):189-207. doi:10.1016/S0065-2571(00)00013-3

85. Acharya S, Sahoo SK. PLGA Nanoparticles Containing Various Anticancer Agents And Tumour Delivery By EPR Effect. *Advanced Drug Delivery Reviews*. 2011;63(3):170-183. doi:10.1016/j.addr.2010.10.008

86. Maeda H, Nakamura H, Fang J. The EPR Effect For Macromolecular Drug Delivery To Solid Tumors: Improvement Of Tumor Uptake, Lowering Of Systemic Toxicity, And

Distinct Tumor Imaging In Vivo. *Advanced Drug Delivery Reviews*. 2013;65(1):71-79. doi:10.1016/j.addr.2012.10.002

87. Hoshyar N, Gray S, Han H, Bao G. The Effect Of Nanoparticle Size On In Vivo Pharmacokinetics And Cellular Interaction. *Nanomedicine (Lond)*. 2016;11(6):673-692. doi:10.2217/nnm.16.5

88. Dreaden EC, Austin LA, Mackey MA, El-Sayed MA. Size matters: Gold Nanoparticles In Targeted Cancer Drug Delivery. *Ther Deliv*. 2012;3(4):457-478.

89. Kulkarni SA, Feng S-S. Effects of Particle Size And Surface Modification On Cellular Uptake And Biodistribution Of Polymeric Nanoparticles For Drug Delivery. *Pharm Res*. 2013;30(10):2512-2522. doi:10.1007/s11095-012-0958-3

90. Kiyose K, Hanaoka K, Oushiki D, et al. Hypoxia-sensitive Fluorescent Probes For In Vivo Real-Time Fluorescence Imaging Of Acute Ischemia. *J Am Chem Soc*. 2010;132(45):15846-15848. doi:10.1021/ja105937q

91. Gilkes DM, Semenza GL, Wirtz D. Hypoxia and the Extracellular Matrix: Drivers Of Tumour Metastasis. *Nat Rev Cancer*. 2014;14(6):430-439. doi:10.1038/nrc3726

92. Cangul H, Salnikow K, Yee H, Zagzag D, Commes T, Costa M. Enhanced Overexpression of an HIF-1/hypoxia-related Protein in Cancer Cells. *Environ Health Perspect*. 2002;110 Suppl 5:783-788. doi:10.1289/ehp.02110s5783

93. Zhong H, De Marzo AM, Laughner E, et al. Overexpression of Hypoxia-Inducible Factor 1alpha In Common Human Cancers And Their Metastases. *Cancer Res*. 1999;59(22):5830-5835.

94. Pampaloni F, Reynaud EG, Stelzer EHK. The Third Dimension Bridges The Gap Between Cell Culture And Live Tissue. *Nat Rev Mol Cell Biol*. 2007;8(10):839-845. doi:10.1038/nrm2236

95. Baker BM, Chen CS. Deconstructing the Third Dimension: How 3d Culture Microenvironments Alter Cellular Cues. *J Cell Sci*. 2012;125(Pt 13):3015-3024. doi:10.1242/jcs.079509

96. Matkar PN, Singh KK, Rudenko D, et al. Novel Regulatory Role Of Neuropilin-1 In Endothelial-To-Mesenchymal Transition And Fibrosis In Pancreatic Ductal Adenocarcinoma. *Oncotarget*. 2016;7(43):69489-69506. doi:10.18632/oncotarget.11060

97. Zhou R, Curry JM, Roy LD, et al. A Novel Association of Neuropilin-1 and MUC1 in Pancreatic Ductal Adenocarcinoma: Role in Induction of VEGF Signaling and Angiogenesis. *Oncogene*. 2016;35(43):5608-5618. doi:10.1038/onc.2015.516

98. Saxena V, Sadoqi M, Shao J. Polymeric Nanoparticulate Delivery System For Indocyanine Green: Biodistribution In Healthy Mice. *International Journal of Pharmaceutics*. 2006;308(1):200-204. doi:10.1016/j.ijpharm.2005.11.003

99. PEG-Intron (Peginterferon alfa-2b) Package Insert. https://www.accessdata.fda.gov/drugsatfda_docs/label/2001/pegsche080701LB.htm. Accessed October 3, 2019.

100. PLEGRIDY (peginterferon beta-1a) injection.

101. Ettinger AR. Pegaspargase (Oncaspar).

102. Working PK, Newman MS, Huang SK, Mayhew E, Vaage J, Lasic DD. Pharmacokinetics, Biodistribution and Therapeutic Efficacy of Doxorubicin Encapsulated in Stealth® Liposomes (Doxil®). *Journal of Liposome Research*. 1994;4(1):667-687. doi:10.3109/08982109409037065

103. Stinchcombe TE, Socinski MA, Walko CM, et al. Phase I and Pharmacokinetic Trial Of Carboplatin And Albumin-Bound Paclitaxel, ABI-007 (Abraxane®) On Three Treatment Schedules In Patients With Solid Tumors. *Cancer Chemother Pharmacol*. 2007;60(5):759-766. doi:10.1007/s00280-007-0423-x

104. Aung NY, Ohe R, Meng H, et al. Specific Neuropilins Expression in Alveolar Macrophages among Tissue-Specific Macrophages. *PLoS ONE*. 2016;11(2):e0147358. doi:10.1371/journal.pone.0147358

105. Wykoff CC, Beasley NJ, Watson PH, et al. Hypoxia-inducible Expression Of Tumor-Associated Carbonic Anhydrases. *Cancer Res*. 2000;60(24):7075-7083.

106. Espey MG, Chen P, Chalmers B, et al. Pharmacologic Ascorbate Synergizes With Gemcitabine In Preclinical Models Of Pancreatic Cancer. *Free Radical Biology and Medicine*. 2011;50(11):1610-1619. doi:10.1016/j.freeradbiomed.2011.03.007

107. Tauchi T, Katagiri S, Okabe S, Tanaka Y, Ohyashiki K. Activity of the Stemness Inhibitor, BBI608, on the Self-Renewal of BCR-ABL1 Positive Leukemia Cells: Molecular Mechanisms. *Blood*. 2014;124(21):905-905.

108. Ben Q, Zheng J, Fei J, et al. High Neuropilin 1 Expression Was Associated With Angiogenesis and Poor Overall Survival in Resected Pancreatic Ductal Adenocarcinoma: *Pancreas*. 2014;43(5):744–749. doi:10.1097/MPA.0000000000000117

109. Pancreatic Cancer - Cancer Stat Facts. https://seer.cancer.gov/statfacts/html/pancreas.html. Accessed May 30, 2018.

110. Perche F, Biswas S, Wang T, Zhu L, Torchilin VP. Hypoxia-targeted siRNA delivery. *Angew Chem Int Ed Engl*. 2014;53(13):3362-3366. doi:10.1002/anie.201308368

111. Mouse : Decision tree for blood sampling | nc3rs. https://nc3rs.org.uk/mouse-decision-tree-blood-sampling. Accessed May 30, 2019.

112. Euhus DM, Hudd C, LaRegina MC, Johnson FE. Tumor Measurement In The Nude Mouse. *J Surg Oncol*. 1986;31(4):229-234.

113. Tomayko MM, Reynolds CP. Determination of Subcutaneous Tumor Size In Athymic (Nude) Mice. *Cancer Chemother Pharmacol*. 1989;24(3):148-154.

114. Street W. Cancer Facts & Figures 2019. 1930:76.

115. Damaskos C, Karatzas T, Nikolidakis L, et al. Histone Deacetylase (HDAC) Inhibitors: Current Evidence for Therapeutic Activities in Pancreatic Cancer. *Anticancer Res*. 2015;35(6):3129-3135.

116. Histone Deacetylases Induce Angiogenesis By Negative Regulation Of Tumor Suppressor Genes | Nature Medicine. https://www.nature.com/articles/nm0401_437. Accessed September 30, 2019.

117. Harbour JW, Dean DC. Chromatin remodeling and Rb activity. *Current Opinion in Cell Biology*. 2000;12(6):685-689. doi:10.1016/S0955-0674(00)00152-6

118. Lee HS, Park SB, Kim SA, et al. A novel HDAC inhibitor, CG200745, Inhibits Pancreatic Cancer Cell Growth And Overcomes Gemcitabine Resistance. *Sci Rep*. 2017;7(1):1-9. doi:10.1038/srep41615

119. Chun S-M, Lee J-Y, Choi J, et al. Epigenetic Modulation With HDAC inhibitor CG200745 Induces Anti-Proliferation In Non-Small Cell Lung Cancer Cells. *PLoS ONE*. 2015;10(3):e0119379. doi:10.1371/journal.pone.0119379

120. Peserico A, Simone C. Physical and Functional HAT/HDAC Interplay Regulates Protein Acetylation Balance. *J Biomed Biotechnol*. 2011;2011:371832. doi:10.1155/2011/371832

121. Singh RK, Cho K, Padi SKR, et al. Mechanism of N-Acylthiourea-mediated Activation of Human Histone Deacetylase 8 (HDAC8) at Molecular and Cellular Levels. *J Biol Chem*. 2015;290(10):6607-6619. doi:10.1074/jbc.M114.600627

122. Gregoretti I, Lee Y-M, Goodson HV. Molecular Evolution of the Histone Deacetylase Family: Functional Implications of Phylogenetic Analysis. *Journal of Molecular Biology*. 2004;338(1):17-31. doi:10.1016/j.jmb.2004.02.006

123. Seto E, Yoshida M. Erasers of Histone Acetylation: The Histone Deacetylase Enzymes. *Cold Spring Harb Perspect Biol*. 2014;6(4):a018713. doi:10.1101/cshperspect.a018713

124. Fischle W, Kiermer V, Dequiedt F, Verdin E. The Emerging Role Of Class Ii Histone Deacetylases. *Biochem Cell Biol*. 2001;79(3):337-348. doi:10.1139/o01-116

125. Histone Deacetylase Inhibitors Suppress Mutant P53 Transcription Via Histone Deacetylase 8 | Oncogene. https://www.nature.com/articles/onc201281. Accessed September 30, 2019.

126. Luo J, Nikolaev AY, Imai S, et al. Negative Control of p53 by Sir2α Promotes Cell Survival under Stress. *Cell*. 2001;107(2):137-148. doi:10.1016/S0092-8674(01)00524-4

127. Deacetylation of p53 Modulates Its Effect On Cell Growth And Apoptosis | Nature. https://www.nature.com/articles/35042612. Accessed September 30, 2019.

128. Decroos C, Bowman CM, Moser J-AS, Christianson KE, Deardorff MA, Christianson DW. Compromised Structure and Function of HDAC8 Mutants Identified in Cornelia de Lange Syndrome Spectrum Disorders. *ACS Chem Biol*. 2014;9(9):2157-2164. doi:10.1021/cb5003762

129. Vaziri H, Dessain SK, Eaton EN, et al. hSIR2SIRT1 Functions as an NAD-Dependent p53 Deacetylase. *Cell*. 2001;107(2):149-159. doi:10.1016/S0092-8674(01)00527-X

130. Histone Deacetylase Inhibitor Augments Anti-Tumor Effect Of Gemcitabine And Pegylated Interferon-A On Pancreatic Cancer Cells | SpringerLink. https://link.springer.com/article/10.1007/s10147-011-0246-y. Accessed September 30, 2019.

131. Dovzhanskiy DI, Arnold SM, Hackert T, et al. Experimental in Vivo And In Vitro Treatment With A New Histone Deacetylase Inhibitor Belinostat Inhibits The Growth Of Pancreatic Cancer. *BMC Cancer*. 2012;12(1):226. doi:10.1186/1471-2407-12-226

132. Combination of HDAC inhibitor TSA and silibinin Induces Cell Cycle Arrest And Apoptosis By Targeting survivin and cyclinB1/Cdk1 in pancreatic cancer cells - ScienceDirect. https://www.sciencedirect.com/science/article/pii/S0753332215002024. Accessed October 1, 2019.

133. Weidle UH, Grossmann A. Inhibition of Histone Deacetylases: A New Strategy To Target Epigenetic Modifications For Anticancer Treatment. *Anticancer Res*. 2000;20(3A):1471-1485.

134. Histone Deacetylase Inhibitors As New Cancer Drugs : Current Opinion in Oncology. https://journals.lww.com/cooncology/fulltext/2001/11000/histone_deacetylase_inhibitors_as_new_cancer_drugs.10.aspx. Accessed October 1, 2019.

135. Structures of a Histone Deacetylase Homologue Bound To The TSA and SAHA inhibitors | Nature. https://www.nature.com/articles/43710. Accessed October 1, 2019.

136. Richon VM, Emiliani S, Verdin E, et al. A Class Of Hybrid Polar Inducers Of Transformed Cell Differentiation Inhibits Histone Deacetylases. *PNAS*. 1998;95(6):3003-3007. doi:10.1073/pnas.95.6.3003

137. Yoshida M, Kijima M, Akita M, Beppu T. Potent and Specific Inhibition Of Mammalian Histone Deacetylase Both In Vivo And In Vitro By Trichostatin A. *J Biol Chem*. 1990;265(28):17174-17179.

138. Singh RK, Mandal T, Balasubramanian N, Cook G, Srivastava DK. Coumarin-suberoylanilide hydroxamic acid as a Fluorescent Probe For Determining Binding Affinities And Off-Rates Of Histone Deacetylase Inhibitors. *Analytical Biochemistry*. 2011;408(2):309-315. doi:10.1016/j.ab.2010.08.040

139. Histone Deacetylase Inhibitors: Molecular Mechanisms Of Action And Clinical Trials As Anti-Cancer Drugs. https://www.ncbi.nlm.nih.gov/pmc/articles/PMC3056563/. Accessed October 1, 2019.

140. Singh RK, Lall N, Leedahl TS, et al. Kinetic and Thermodynamic Rationale for Suberoylanilide Hydroxamic Acid Being a Preferential Human Histone Deacetylase 8 Inhibitor As Compared to the Structurally Similar Ligand, Trichostatin A. *Biochemistry*. 2013;52(45):8139-8149. doi:10.1021/bi400740x

141. Singh RK, Suzuki T, Mandal T, et al. Thermodynamics of Binding of Structurally Similar Ligands to Histone Deacetylase 8 Sheds Light on Challenges in the Rational Design of Potent and Isozyme-Selective Inhibitors of the Enzyme. *Biochemistry*. 2014;53(48):7445-7458. doi:10.1021/bi500711x

142. Phiel CJ, Zhang F, Huang EY, Guenther MG, Lazar MA, Klein PS. Histone Deacetylase Is a Direct Target of Valproic Acid, a Potent Anticonvulsant, Mood Stabilizer, and Teratogen. *J Biol Chem*. 2001;276(39):36734-36741. doi:10.1074/jbc.M101287200

143. Promising antitumor activity with MGCD0103, a novel isotype-selective histone deacetylase inhibitor: Expert Opinion on Investigational Drugs: Vol 17, No 8. https://www.tandfonline.com/doi/abs/10.1517/13543784.17.8.1247. Accessed October 1, 2019.

144. Valproic acid defines a novel class of HDAC inhibitors inducing differentiation of transformed cells | The EMBO Journal. https://www.embopress.org/doi/full/10.1093/emboj/20.24.6969. Accessed October 1, 2019.

145. Histone Deacetylase Inhibitors Trigger a G2 Checkpoint in Normal Cells That Is Defective in Tumor Cells | Molecular Biology of the Cell. https://www.molbiolcell.org/doi/full/10.1091/mbc.11.6.2069. Accessed October 1, 2019.

146. Histone Deacetylase Inhibitor Selectively Induces p21WAF1 Expression And Gene-Associated Histone Acetylation | PNAS. https://www.pnas.org/content/97/18/10014.short. Accessed October 1, 2019.

147. Sandor V, Senderowicz A, Mertins S, et al. P21-dependent G 1 Arrest With Downregulation Of Cyclin D1 and Upregulation Of Cyclin E by the Histone Deacetylase inhibitor FR901228. *Br J Cancer*. 2000;83(6):817-825. doi:10.1054/bjoc.2000.1327

148. The Histone Deacetylase Inhibitor And Chemotherapeutic Agent Suberoylanilide Hydroxamic Acid (SAHA) Induces A Cell-Death Pathway Characterized By Cleavage Of Bid And Production Of Reactive Oxygen Species | PNAS. https://www.pnas.org/content/98/19/10833.short. Accessed October 1, 2019.

149. Up-Regulation Of Costimulatory/Adhesion Molecules By Histone Deacetylase Inhibitors In Acute Myeloid Leukemia Cells | Blood Journal.

150. Goswami U, Kandimalla R, Kalita S, Chattopadhyay A, Ghosh SS. Polyethylene Glycol-Encapsulated Histone Deacetylase Inhibitor Drug-Composite Nanoparticles for Combination Therapy with Artesunate. *ACS Omega*. 2018;3(9):11504-11516. doi:10.1021/acsomega.8b02105

151. Denis I, el Bahhaj F, Collette F, et al. Histone deacetylase Inhibitor-Polymer Conjugate Nanoparticles For Acid-Responsive Drug Delivery. *European Journal of Medicinal Chemistry*. 2015;95:369-376. doi:10.1016/j.ejmech.2015.03.037

152. Thoma G, Patton JT, Magnani JL, Ernst B, Öhrlein R, Duthaler RO. Versatile Functionalization of Polylysine: Synthesis, Characterization, and Use of Neoglycoconjugates. *J Am Chem Soc*. 1999;121(25):5919-5929. doi:10.1021/ja984183p

153. Troll W, Cannan RK. A Modified Photometric Ninhydrin Method For The Analysis Of Amino And Imino Acids. *Journal of Biological Chemistry*. 1953;200:803-811.

154. Suppression of Prostate Cancer Progression By Cancer Cell Stemness Inhibitor Napabucasin - Zhang - 2016 - Cancer Medicine - Wiley Online Library. https://onlinelibrary.wiley.com/doi/full/10.1002/cam4.675. Accessed October 1, 2019.

155. Bubna AK. Vorinostat—An Overview. *Indian J Dermatol*. 2015;60(4):419. doi:10.4103/0019-5154.160511

156. Shah RR. Safety and Tolerability of Histone Deacetylase (HDAC) Inhibitors in Oncology. *Drug Saf*. 2019;42(2):235-245. doi:10.1007/s40264-018-0773-9

157. Balasubramanian S, Ramos J, Luo W, Sirisawad M, Verner E, Buggy JJ. A Novel Histone Deacetylase 8 (HDAC8)-Specific Inhibitor PCI-34051 Induces Apoptosis in T-cell lymphomas. *Leukemia*. 2008;22(5):1026-1034. doi:10.1038/leu.2008.9

158. Gong J, Xie J, Bedolla R, et al. Combined targeting of Stat3/NFκB/Cox-2/EP4 for Effective Management Of Pancreatic Cancer. *Clin Cancer Res*. 2014;20(5):1259-1273. doi:10.1158/1078-0432.CCR-13-1664

159. Kang Y, Nian H, Rajendran P, et al. HDAC8 and STAT3 repress BMF Gene Activity In Colon Cancer Cells. *Cell Death Dis*. 2014;5(10):e1476. doi:10.1038/cddis.2014.422

160. Ray P, Alhalhooly L, Ghosh A, et al. Size-Transformable, Multifunctional Nanoparticles from Hyperbranched Polymers for Environment-Specific Therapeutic Delivery. *ACS Biomater Sci Eng*. 2019;5(3):1354-1365. doi:10.1021/acsbiomaterials.8b01608

161. Colombo AP, Briançon S, Lieto J, Fessi H. Project, Design, and Use of a Pilot Plant for Nanocapsule Production. *Drug Development and Industrial Pharmacy*. 2001;27(10):1063-1072. doi:10.1081/DDC-100108369

162. Galindo-Rodríguez SA, Puel F, Briançon S, Allémann E, Doelker E, Fessi H. Comparative Scale-Up Of Three Methods For Producing Ibuprofen-Loaded Nanoparticles. *European Journal of Pharmaceutical Sciences*. 2005;25(4):357-367. doi:10.1016/j.ejps.2005.03.013

APPENDIX

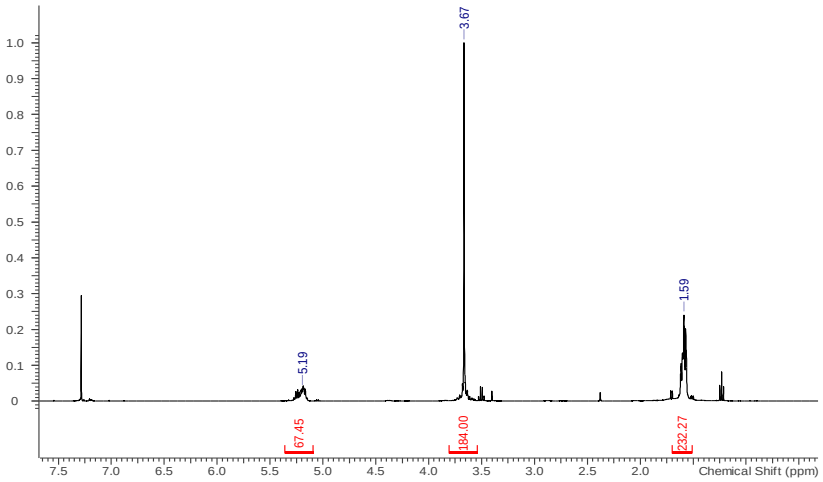

Figure A1. ^{1}H NMR hypoxia-responsive polymer PEG$_{2000}$ –diazobenzene–PLA$_{6000}$.

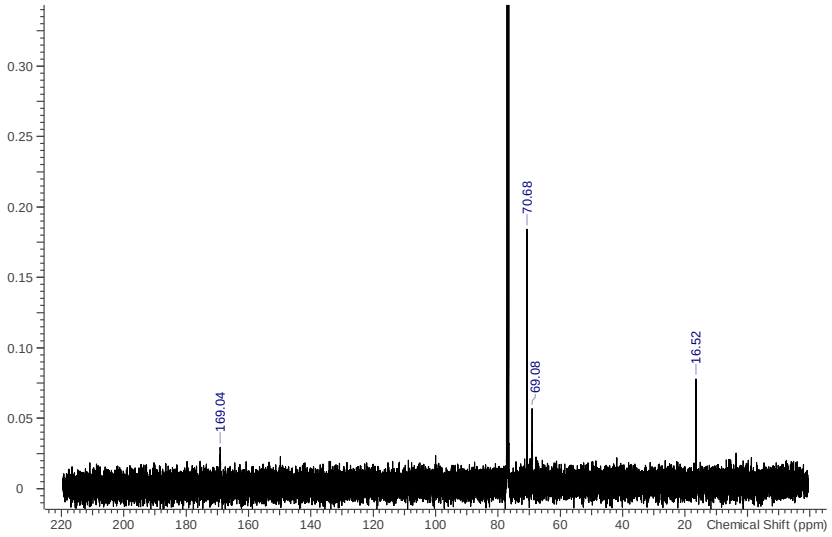

169.04 ((-CH-**C**=O)), 69.08 ((-**C**H-C=O)), 70.68 ((CH2-CH2-O)), 16.52 ((**C**H3-CH-C=O))

Figure A2. ^{13}C NMR in CDCl$_3$ hypoxia-polymer PEG$_{2000}$–diazobenzene–PLA$_{6000}$.

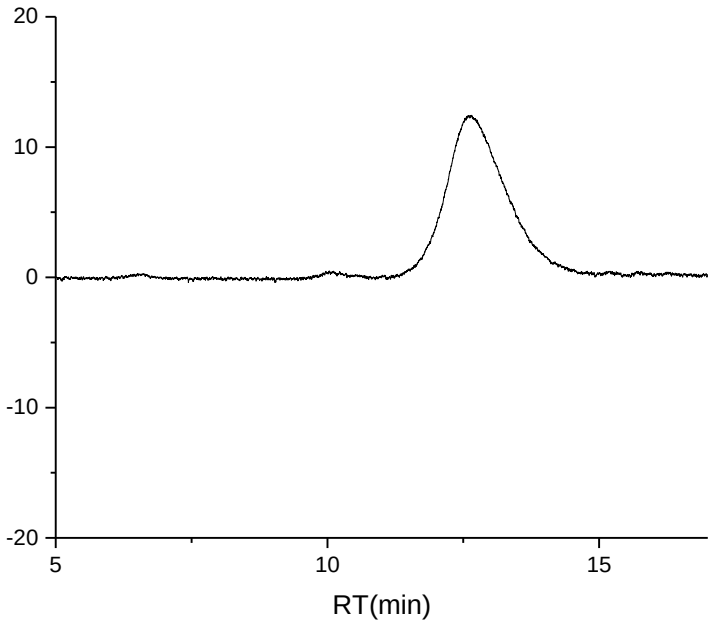

Mn	5,580	Mw	6,451
Mz	7,391	Mz+1	8.459
Mv	6,451	Mp	6,535
Mz/Mw	1.147	Mw/Mn (PDI)	1.156

Figure A3. GPC in THF Hypoxia-Polymer PEG_{2000}–Diazobenzene–PLA_{6000}.

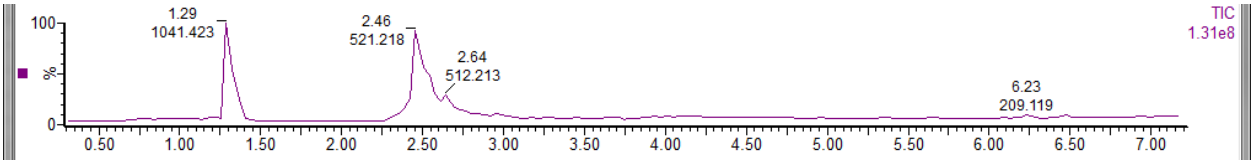

RT=2.46, base peak 521.218 is a double charged 1041.423

Figure A4. iRGD Peptide Mass Spectrometry.

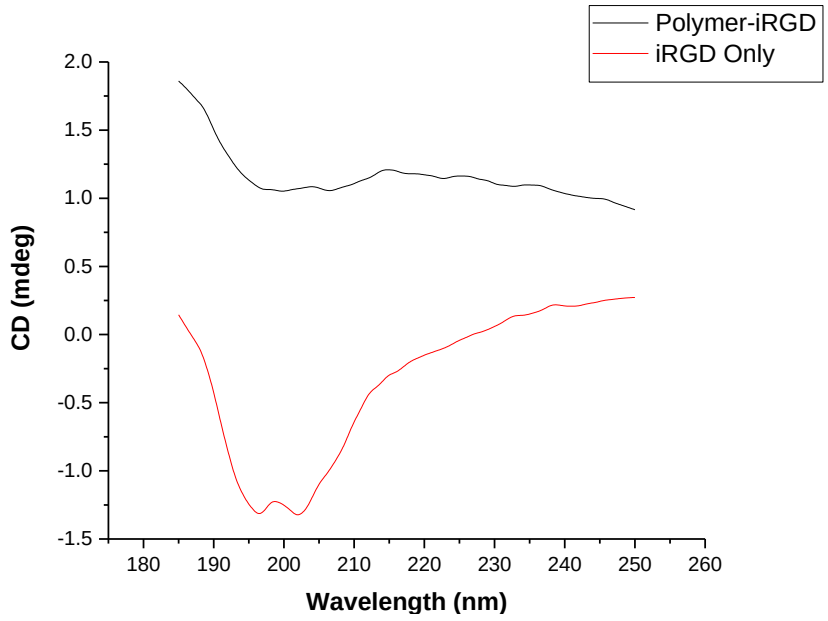

Figure A5. iRGD-Polymer Conjugate Circular Dichroism.

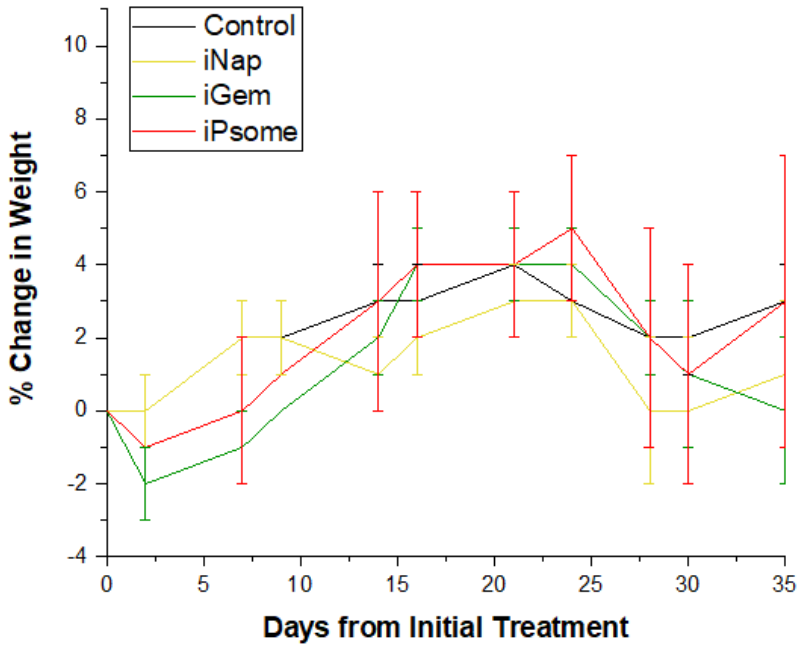

Figure A6. Mouse Weight (Polymersomes Treatments).

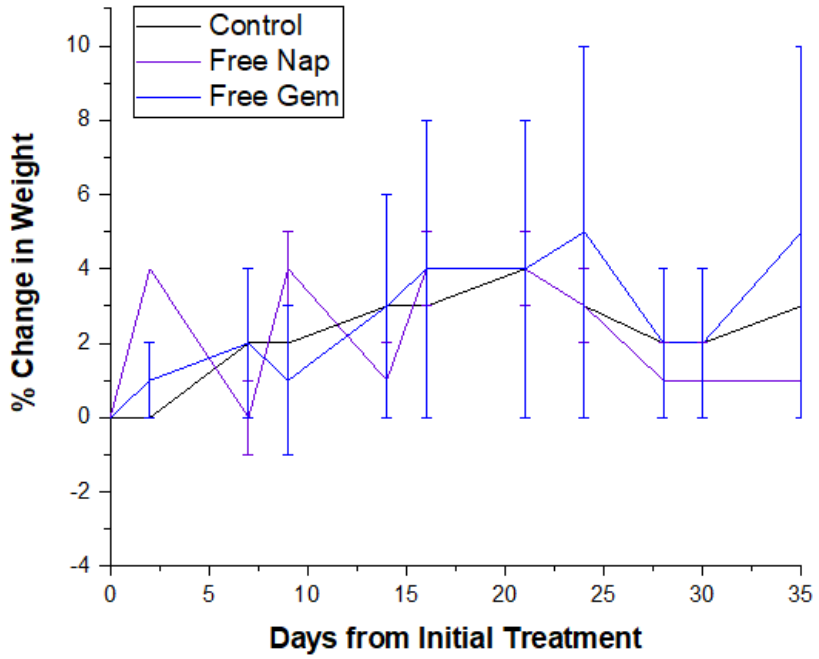

Figure A7. Mouse Weight (Free Unencapsulated Treatments).

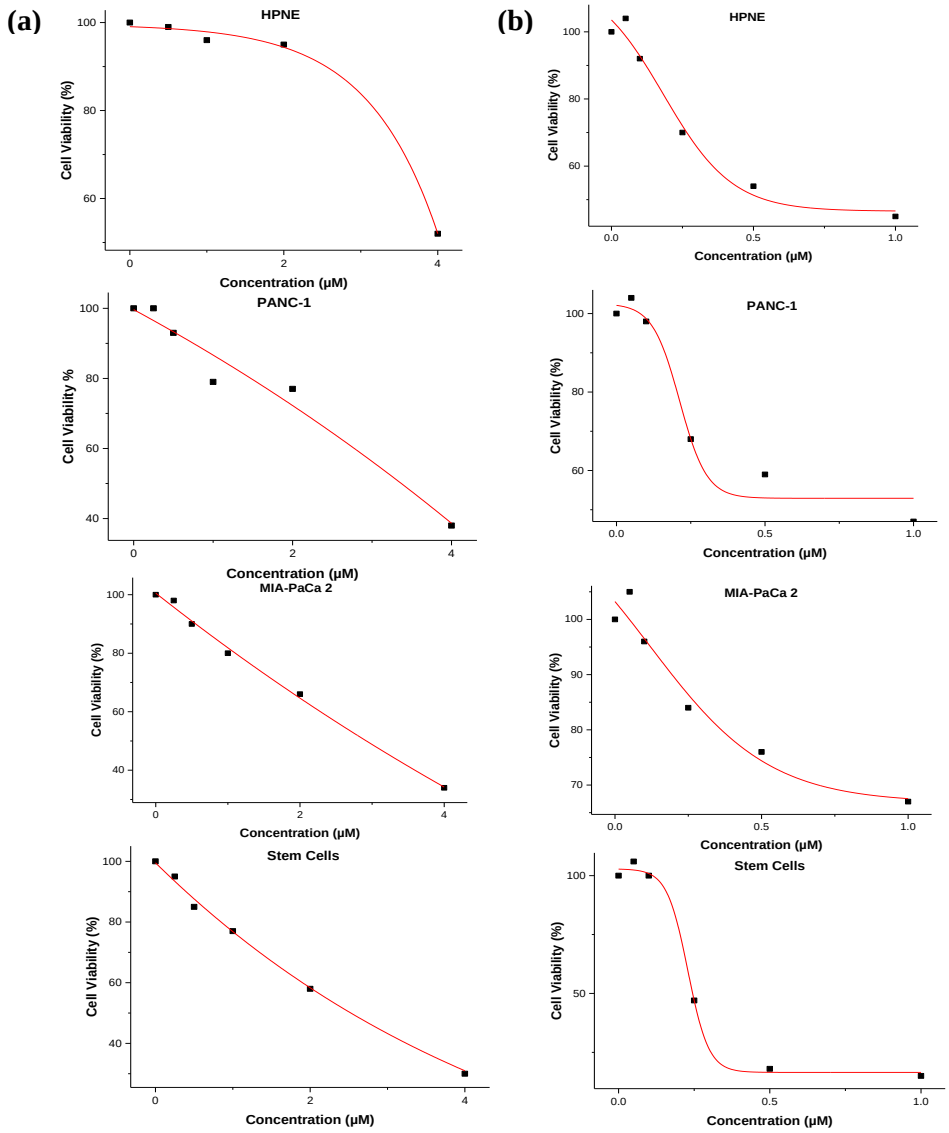

Figure A8. Dose-Response Curves. Dose-response curves for the four different cell lines are shown. Column (a) represents each cell type exposed to free napabucasin given in doses ranging from 0 μm up to 4 μm. Column (b) represents each cell type exposed to HDAC8 responsive nanoparticles with varying concentrations of encapsulated napabucasin ranging from 0 nm up to 1 μm.